Self-Assembled Chitin Nanofibers: Properties and Applications

Pegah Hassanzadeh

A dissertation

submitted in partial fulfillment of the

requirements for the degree of

Doctor of Philosophy

University of Washington

2015

Reading Committee:

Marco Rolandi, Chair

Mehmet Sarikaya

Dwayne Arola

Program Authorized to Offer Degree:

Materials Science and Engineering

University of Washington

Abstract

Self-assembled Chitin Nanofibers: Properties and Applications

Pegah Hassanzadeh

Chair of the Supervisory Committee:
Associate Professor Marco Rolandi
Department of Materials Science and Engineering

Bio-inspired materials offer intrinsic properties such as biodegradability and biocompatibility. These properties make these materials strong candidates for a variety of applications such as biomedical, textile, filtration, packaging and food applications. Among these materials, chitin, the second most abundant polysaccharide after cellulose, is a very attractive material. It is the main structural component of exoskeletons or the cuticles of many invertebrates and has many desirable properties. However, chitin is insoluble in most organic solvents, which limits its practical use. Our group has demonstrated a novel method of developing self-assembled ultrathin chitin nanofibers from the solution of squid pen β-chitin in hexafluoroisopropanol (HFIP). Based on this method, I have developed different techniques to fabricate high quality chitin films and studied the process-structure-property relationship in these films. Based upon the knowledge I obtained from this study, I have fabricated flexible, yet sturdy micropatterned chitin substrates with desirable microstructure and mechanical properties for tissue engineering, specifically myocardial tissue engineering. These substrates show no cytotoxicity and great mechanical stability in the wet condition of cell culture. Focusing on the mechanical properties of these substrates and getting inspired by nature, I have based my next work upon enhancing these

properties by mixing chitin nanofibers and silk fibroin to make chitin-silk biocomposites. The mechanical properties of these biocomposites enhances with respect to chitin and silk alone due to strong hydrogen bonding between two molecules. Based on this study, I have shown the self-assembly of chitin nanofibers in the matrix of another natural component, GelMA, a functionalized gelatin and collagen derivative. This GelMA-chitin biocomposites offer outstanding properties such as high strength and extensibility and also great biocompatibility and vasculogenic activity. In this way, throughout the course of my PhD, I have accomplished developing innovative bio-inspired nanofiber biomaterials with great biological, physical and mechanical properties to be used in biomedical applications. The outlook of my research is to replace HFIP with more green solvents preferably water systems. HFIP is a volatile corrosive liquid that can cause burns and respiratory problems in human. Using water systems to self-assemble chitin nanofibers leads to establishment of environmentally-friendly process to make nanofiber films with great strength and stiffness and high surface area using only natural green materials and processes and with causing no harmful waste.

TABLE OF CONTENTS

LIST OF FIGURES

LIST OF TABLES

ACKNOWLEDGEMENTS

First, I would like to express my deepest gratitude toward my great advisor and mentor, Prof. Marco Rolandi, who expertly guided me through my graduate education. I really appreciate all his constructive comments and guidance and also non-stop support throughout my entire PhD. His unwavering enthusiasm for science and exploration of new approaches has been always inspiring and encouraging for me. His advice, support and novel perspectives made my journey at University of Washington very enjoyable.

Second, I am grateful to my PhD committee members, Prof. Sarikaya, Prof. Arola and Prof. Lalic, for all their comments and suggestions, which definitely added more value to this work. I would also like to thank our collaborators, Prof. Khademhosseini in Harvard University, Prof. Annabi in Northeastern University, Prof. Omenetto in Tuft University, and Prof. Cross in Trinity College of Dublin, Ireland, for their contributions to this work. Also, I am grateful to Office of Naval Research (ONR) to fund my research throughout my PhD.

My wonderful husband, Mohammad Haghighipanah, deserves a special mention for his endless and non-stop support. He blessed me with a life of joy and stood by me through this journey's ups and downs. I am indebted to him and cannot thank him enough for his boundless emotional support.

I would also love to express my deep appreciation towards my amazing parents for their inseparable support. They have raised me, loved me, and supported me all through my life. They provided a suitable environment for me to study, encouraged me to pursue this degree, and supported me financially and emotionally. Likewise, special thanks to my amazing brother, Dr. Pedram Hassanzadeh, for all his encouragement and care during my PhD studies and also throughout my life. He has been a great inspiration for me in every aspect of my life. I am so blessed by unconditional love and support from my husband and all my family members.

Furthermore, I am grateful to all members of Rolandi Research Group at University of Washington and all my great friends in Seattle and all over the world for their scientific contributions and endless emotional support.

Chapter 1. INTRODUCTION

1.1 CHITIN AND CHITOSAN, CHEMISTRY AND PROPERTIES

In the last decade, naturally derived polymers have been gaining a lot of attentions for wide range of applications such as agriculture, food industry, paper making and textile industry, packaging, biomedicine and pharmaceuticals due to their wide range of great properties.[5] Biopolymers such as polysaccharides, a natural component of living organisms, are intrinsically renewable, biodegradable and biocompatible, which make them attractive for many scientists.[5] Among polysaccharides, chitin and chitosan have been materials of interest for many years because of their sustainability, biocompatibility, biodegradability and accessibility.[6, 7] They have been categorized as "nature's most versatile biomaterial".[8] The main interest in chitin began in the 1920s, when market demanded low cost fibers. Back then, many attempts were made to solubilize chitin. However, the discovery of nylon in the late 1930s and invention of synthetic polymer fibers slowed down chitin research.[9, 10] In the 1970s, researchers resumed their research on chitin and discovered many interesting properties of chitin and chitosan.[10]

Chitin is the second most abundant polysaccharide (aminopolyglucan) in nature after cellulose. It is the main biomass resource with more than 10^{11} tons per year production in nature.[11] It is composed of long linear chains of β(1-4)-linked *N*-acetyl-D-glucosamine residues (Figure 1.1a).[1, 4] In nature, it is found as semi-crystalline nanofibers with hydrophobic interaction between glucosamine rings and hydrogen bonding along the linear chains.[6] The repeating unit of chitin contains a hexose ring including an oxygen as part of the ring with an acetamido group at the second carbon position, united together by β-glycosidic bonds.[1] It is a structural material found in the exoskeletons or the cuticles of many invertebrates and in the cell walls of green algae, some fungi and yeasts.[1, 12] This poly-N-acetyl glucosamine exhibits structural similarity to cellulose with a repeating unit of β(1-4)-linked D-glucose (Figure 1.1b), differing only in the replacement of C-2 hydroxyl residues by acetamido groups.[9] Chitin can exist in different degree of deacetylation depending on the polysaccharide source and isolation conditions. Chitin is not soluble in water, diluted acid/base solutions and most organic solvents due to its tight rigid crystalline structure. This structure originates from the strong bonds between the acetamido group, hydroxyl group and carbonyl group inside and in-between the chains of chitin.[6, 7, 11] As a

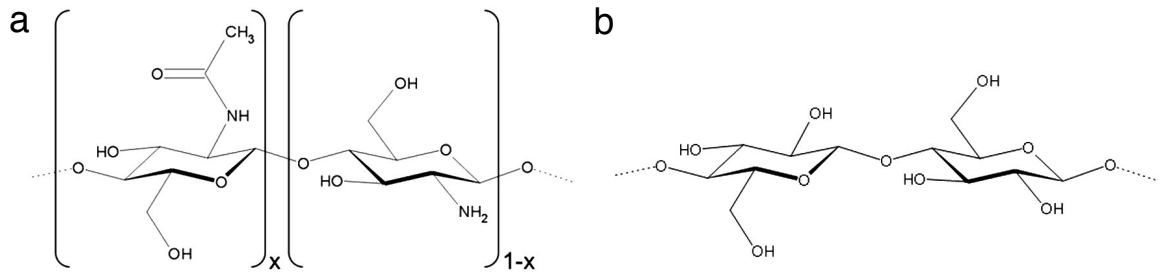

Figure 1.1. Chemical structure of (a) Chitin when x > 0.5 or chitosan when x < 0.5, (b) Cellulose.[1]

result, chitin is relatively difficult to process and due to its insolubility in aqueous solution, has become less accessible for researcher and scientists.[13] Chitin dissolves in strong acids such as dichloroacetic acid and trichloroacetic acid[8] as well as highly polar fluorinated solvents such as hexafluoroisopropanol[8] or hexafluoroacetone.[5] Also, recently, calcium solvents have been shown to dissolve chitin in mild conditions.[7] Some other solvents systems such as concentrated H_2SO_4 or HCl, LiSCN/H_2O, chloroethanol/H_2SO_4, trichloroacetic acid, urea/NaOH, and ionic liquids have been reported to dissolve chitin as well. However, all these solvents have their own limitations such as toxicity, being corrosive, degradative effect on the chitin polymer, high costs and not being environmentally friendly.[14]

The most common derivative of chitin, chitosan, is produced by chitin partial deacetylation with concentrated alkali solutions at elevated temperatures. Chitin and chitosan are effectively the same macromolecule entity, varying only in the fraction of acetylated repeating (Figure 1.1a).[1] In Figure 1.1a, x is the degree of acetylation, defined as the mole ratio of acetylated repeating units over that of the total repeating units. Deacetylation is never complete in practice, which implies that chitosan obtained from commercial sources is chitin with a very low degree of acetylation (typically x=0.1 to 0.35).[1] Chitosan has rigid D-glucosamine structures characterize by high crystallinity and hydrogen bonding capacity, which justifies its poor solubility in common organic solvents and complete insolubility in aqueous solutions with the pH value above 7. Reducing the molecular weight and decreasing the crystallinity amount by random deacetylation improve its solubility in dilute acids below pH 6.4 due to protonation of free primary amines and formation of soluble polybase-acid complex.[6] Due to two types of active groups of chitosan, the free amino groups on the deacetylated units and hydroxyl groups on the C3 and C6 carbons on both acetylated and deacetylated units, this material is easier to use and more malleable for

processing than chitin.[1]

Similar to cellulose, chitin can exist in different polymorphic forms, α- and β-chitin. In both forms, intra-sheet hydrogen bonds keep the chitin chains tightly inside the sheet. These hydrogen bonds are mainly between CO and NH groups. In α-chitin, there are some inter-sheet hydrogen bonds as well, which are not found in β-chitin. The chitin chains are antiparallel in α-chitin and parallel in β-chitin (Figure 1.2).[4, 6] Usually, the outer skeletal is chitin in the form of α, while β-chitin can be found in squid pen and some diatoms.[1, 7] The weaker hydrogen bonding between the chains of β-chitin may count for its higher reactivity. In addition, β-chitin has the unique characteristic of encompassing small molecules including water into its crystal lattice; so, it becomes hydrated and swollen easily in water.[1]

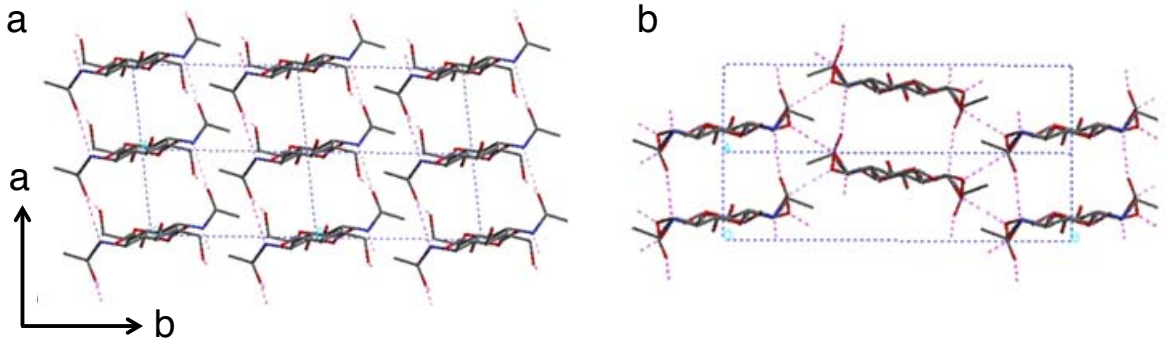

Figure 1.2. Structure of chitin polymorphs, (a) β-chitin, (b) α-chitin.[4]

1.2 CHITIN IN NATURE

Chitin exists in the form of nanofiber arrangements in living organisms because of its high crystallinity and linear structure.[15] These nanofibers basically form a complex hierarchical organization with or without other polysaccharides and proteins.[3] As an example, in crustacean shells, at the molecular level, 3-nm long-chain chitin nanofibers held by strong hydrogen bonding are wrapped with silk-like protein and assemble into 60 nm fibers (Figure 1.3). These fibers further assemble to bundles. The bundles then align and form horizontal sheets, which are stacked in a helicoid fashion, creating a twisted plywood structure. A stack of layers that have full 180° rotations with respect to each other is referred to as a Bouligand Structure.[16] This Bouligand structure demonstrates highly anisotropic mechanical properties.[3] The nanofiber structure renders the material with very high tensile strength, high chemical resistance, and excellent environmental properties.[14] As a result, reproducing these structures can be very attractive for many applications.

Researchers have tried to engineer composites with functions similar to those found in biological materials. If we use the biological systems as a source of inspiration, then more manmade materials might display these unique architectural features and thus multifunctional performance

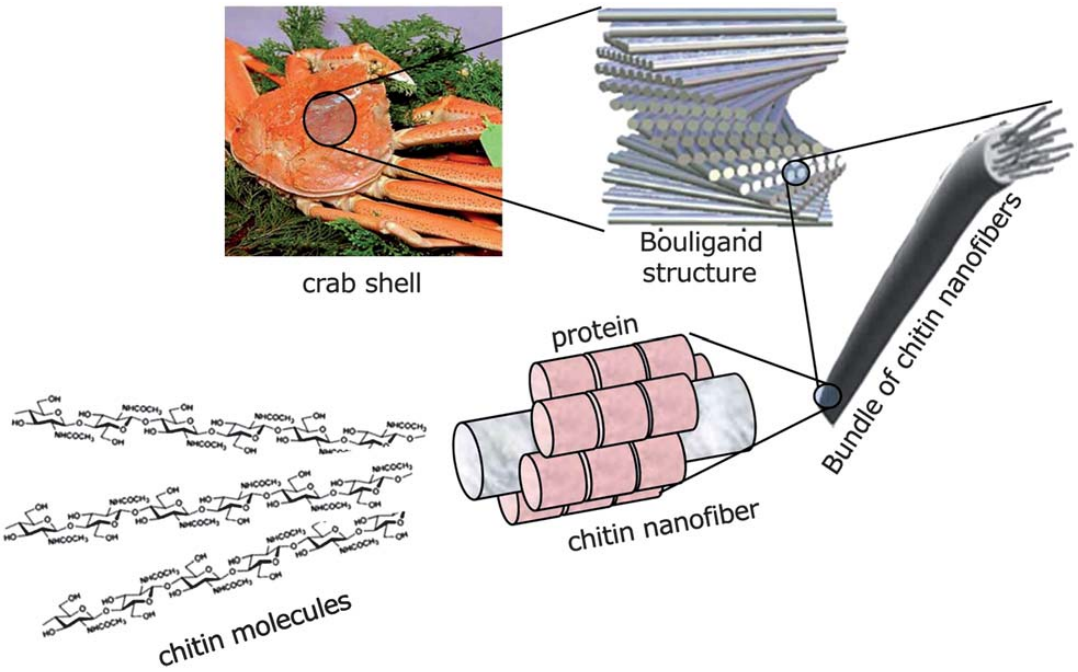

Figure 1.3. Hierarchical structure of the exoskeleton structure of crab shells.[3]

characteristics. There are two approaches to achieve this goal of bio-inspired processing, Biomimetics and Bioduplication. The biomimetic approach aims at designing hierarchical structures by synthesis and processing methods, which are very artificial compared to the biological mechanisms. However, the resulting artificially engineered composites will show structural features similar to those found in biological systems. Conversely, the bioduplication uses the very similar mechanisms to biological ones to reproduce the desirable natural features and properties.[17]

1.3 Approaches to Make Chitin Nanofibers

Over the years, people have been trying to prepare chitin nanofibers having two motivations: First, to mimic the nature and exploit the exceptional intrinsic biological properties and functionality of it and second, to create synthetic materials containing nanofibers (fiber diameter less than 100 nm), which renders the material with a characteristic morphology, high surface to volume ratio and unique optical and mechanical properties. Various synthetic methods have been utilized such as acid hydrolysis, Tempo-mediated oxidation, ultrasonication, electrospinning, mechanical treatment, and gelation.[11] All these methods have their own limitations such as harsh conditions of processing (highly acidic or basic), which result in depolymerization and deacetylation of chitin, pricing and complexity.

The very common and widely-used method to make chitin/chitosan nanofibers is electrospinning.[18] This method produce fibers from a polymer solution using interactions between fluid dynamics and electrically charged surfaces and liquids.[3] However, the resulting nanofibers obtained from this method have large diameters, not similar to nature.[19] Smaller nanofibers existing in nature is difficult to produce. It has been also reported that self-assembly is a common route for synthesis of many bio-inspired nanofibers; however, water insolubility of chitin impedes the use of this approach.[20] Processing of chitin has been always challenging because of the strong bonds, which renders the material with water insolubility and unreactivity.

1.4 Self Assembly of Chitin Nanofibers

Chitin is an abundant biodegradable polysaccharide with outstanding properties such as biocompatibility, nontoxicity, sustainability, mechanical stability and antibacterial properties. These properties make chitin and its derivatives as perfect candidates for many applications such as wound dressing and sutures,[10] microneedle for diagnostics,[21] tissue engineering scaffolds,[4, 5, 22, 23] biocompatible devices,[24, 25] water filtration, cosmetic, agriculture, food industries,[7] and crop protection.[12] All these fantastic properties and potential applications have motivated our group to explore the alternative methods to process chitin. In 2009, we developed a novel method to produce chitin nanofibers *in vitro* in mild conditions by self-assembly to be able to use it for different applications later on.[26] In this method, the solution of squid pen β-chitin in hexafluoroisopropanol (HFIP), a chitin nanofiber ink, self-assembles into ultrathin (3 nm) α-chitin nanofibers upon drying. The diameter of these chitin nanofibers (*ca.* 3 nm) is close to the one of natural biogenic chitin (Figure 1.4). This diameter is relatively insensitive to processing conditions including the concentration of the initial chitin solution or ink, possibly because nanofibers with 3 nm diameter are the thermodynamically the most stable form.[26] Chitosan does not form nanofibers because it lacks chitin's acetylamide groups that contribute to hydrogen bonding during the chitin nanofiber self-assembly process.

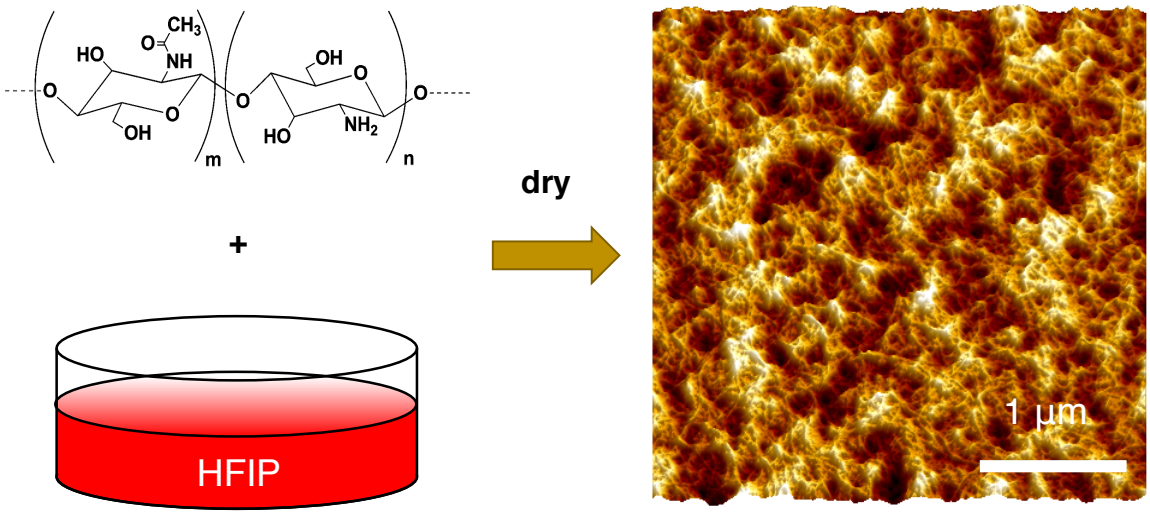

Figure 1.4. Self-assembly of ultrathin chitin nanofiber from the chitin/HFIP solution upon drying.

1.5 OBJECTIVE OF THIS THESIS

The objective of my PhD research is to further study and characterize the process of self-assembly of chitin nanofibers developed by our group. This method is using synthetic means to create biomaterials based on chitin and regenerate its chemical and natural biological functions and properties. Furthermore, I explore the potential applications of this self-assembled chitin nanofiber films in different fields including biomedical.

First, I study the structure-property-processing relationship of chitin nanofiber network. The property investigated is mechanical properties in macroscale and microscale. The results of this study, mechanical properties of self-assembled chitin nanofiber networks, are reported in Chapter 2 showing a robust tunability of final mechanical properties of chitin films based on processing and microstructure of samples.

In Chapter 3, I show the application of micropatterned chitin substrates in tissue engineering. Here, I utilize the developed method by our group combined with replica molding to produce transparent, ultra–thin (<10 μm), mechanically robust, yet flexible self-assembled chitin nanofiber micropatterned substrates for tissue engineering. With these micropatterned substrates, I demonstrate cell sheets of aligned fibroblasts as a proof of concept that chitin substrates are non-cytotoxic and biocompatible. The supported cell sheets made in this manner are mechanically robust and easy to handle, yet flexible and bendable in the shape of choice.

Furthermore, in Chapter 4, I introduce a bio-inspired composite from the solution of co-assembly of ultrafine (3 nm) chitin nanofibers in a silk fibroin matrix. This work is the first attempt of our group to mimic the composition of organic part of natural structural materials. With the ease of solution processing, natural abundance of the material constituents, and biodegradability, I develop chitin-silk biocomposite, which may find applications in naturally-derived plastics as well as biomedical devices.

In the next step, in Chapter 5, I demonstrate the possibility of self-assembly of chitin nanofibers in the matrix of collagen, another natural protein. Again, motivation for this study is also mimicking the nature and obtaining more insight into chitin-protein interactions in natural structural materials. In this work, I reinforce gelatin (collagen derivative)-based hydrogels, gelatin methacryloyl (GelMA), with self-assembled chitin nanofibers in order to make ultrastrong flexible hybrid hydrogels for tissue engineering applications. These hydrogels offer

broad advantages of combined gelatin-based hydrogels and chitin nanofibers such as low cost, abundance of initial components, ease of production and natural cell binding and promoting properties as well as high strength, stiffness and flexibility due to the existence of the chitin nanofibers as a reinforcement agent. The co-existence of high stiffness and flexibility make these hydrogels unique for tissue engineering and vascular grafting.

Chapter 2. MECHANICAL PROPERTIES OF SELF-ASSEMBLED CHITIN NANOFIBER NETWORKS [27]

2.1 INTRODUCTION

In this work, I have studied the structure-property-processing relationship of chitin nanofiber network structures self-assembled from drying a solution of squid pen β-chitin in HFIP (Figure 2.1a).[26] I showed that processing method, drying time, and solution concentration affect chitin nanofiber network morphology, density, and consequently the mechanical properties of bulk films. In addition to simple Drop Casting (DC) method (Figure 2.1a),[26] I explored three new processing methods in an attempt to gain better control of chitin nanofiber network morphology and properties.

2.2 FABRICATION METHODS

Cold-Press (CP), Vacuum Drying (VD), and Vacuum-assisted Filtration (VF)[28] (Figure 2.1b, c, and d) were used with chitin-HFIP solutions of 0.4% (w/v) and 0.8% (w/v). For CP, the initial solutions were dried for 3-5 days in air until a gel consistency was reached. The gel was then compressed between two microscope slides (Figure 2.1b). After approximately 2 additional days of drying, flat and transparent chitin films were obtained. In order to expedite the chitin network formation process, I produced drop cast films under vacuum drying. VD reduced drying time to approximately 2-3 days (Figure 2.1c). In VF (Figure 2.1d), the chitin-HFIP solution was supported on a filter paper coated with a thin layer of Polydimethylsiloxoane (PDMS) while drying. The PDMS coated filter paper was placed in a porcelain funnel connected to the house vacuum and covered with a glass cover in order to minimize evaporation from the top. The chitin films dried in approximately 1 day. For all processing methods, chitin nanofibers were self-assembled for both the 0.4% (w/v) and the 0.8% (w/v) concentrations (Figure 2.1e-j). The films from CP had apparent higher surface roughness for both concentrations. This higher roughness was likely due to the chitin films replicating the hard filter surface. In contrast, the VF films were smooth. The morphology of the VD films includes larger diameter fibers for 0.4% (w/v) concentration, while the morphology at 0.8% (w/v) was similar to the morphology of VF films. The fibers from VD at 0.4 %(w/v) were similar in appearance to the fibers from LiCl/DMAC

precipitation in water previously observed.[26] It is possible that with the faster drying times associated with the VD films, the fibers may assemble into thicker bundles rather than creating a uniform smaller network. For all methods, initial surface morphology inspection suggests that the films from the solution with higher concentration (0.8 % (w/v)) are denser than the films made from the solution with lower concentration (0.4 % (w/v)).

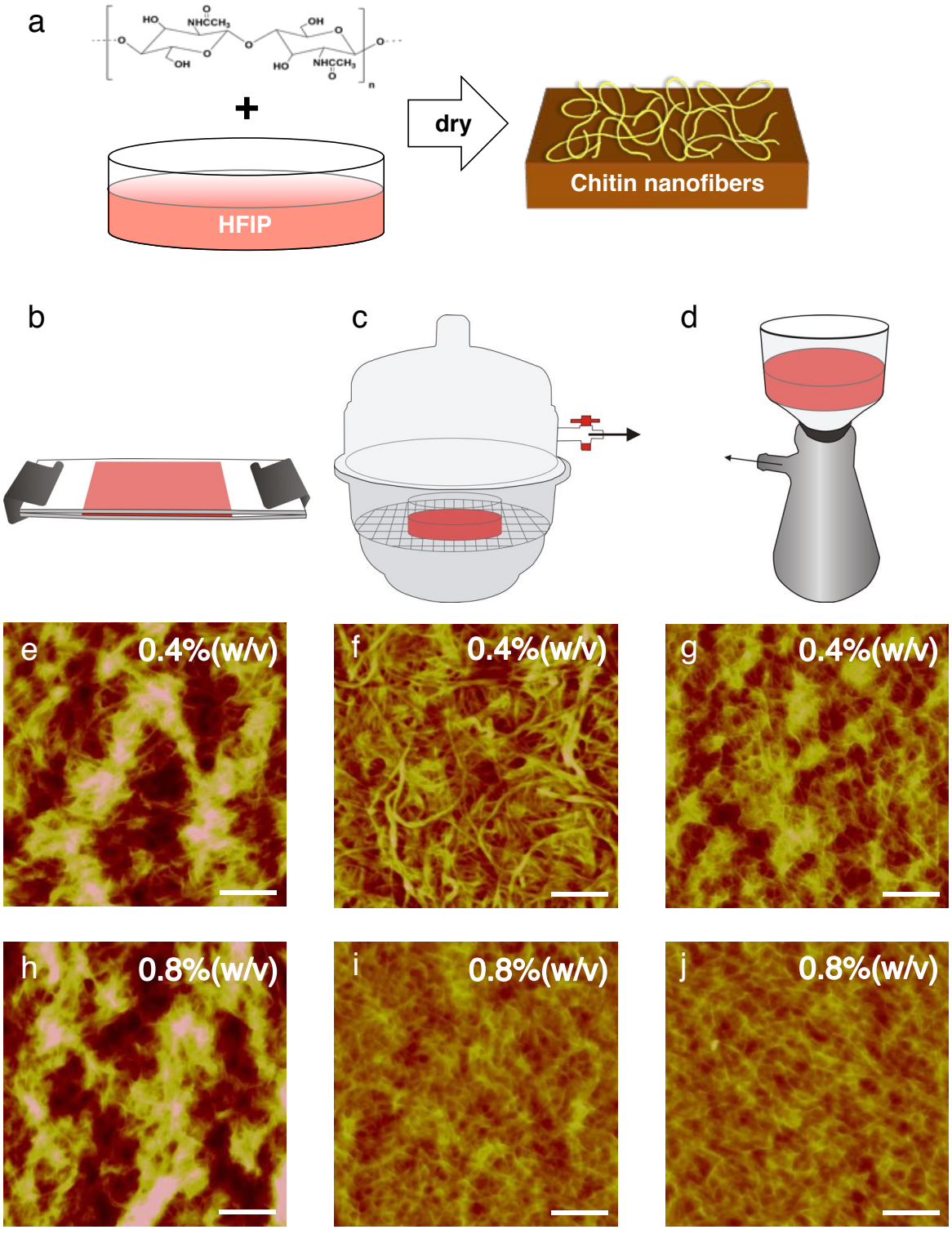

Figure 2.1. Schematic illustration for the self-assembly process of the chitin nanofibers by different methods (a) Simple drop casting method (b) Cold-Press method (CP) (c) Vacuum Drying method (VD) (d) Vacuum-assisted Filtration method (VF) (e-g) AFM images for 0.4% (w/v) chitin/HFIP solution prepared by CP, VD, and VF, respectively. (h-j) The AFM images for 0.8% (w/v) chitin/HFIP solution prepared by CP, VD, and VF, respectively. Scale bars are 200 nm.

2.3 MATERIALS CHARACTERIZATION

To confirm this conjecture, I measured the density of the films by comparing the weight of small film samples of the same size (Figure 2.2a). For a given solution concentration, all the processing methods resulted in films with different density smaller than the density of solid chitin (1.43 g/cm^3). The concentration of the initial chitin/HFIP solution used for self-assembly affected the density of the films obtained from CP and VD with higher solution concentration yielding films with higher density. The same effect was not observed for VF films and film density did not change as a function of initial solution concentration. For shorter drying time, once the solution reached the critical concentration for fiber self-assembly, the nanofiber network may have frozen into place regardless of initial solution concentration. For slower drying time, nanofibers might form at a broader range of concentrations and films from solution of higher concentration may result in denser nanofiber network.

In order to study whether the different methods affected the crystalline structure of the chitin nanofibers, I used X-Ray Diffraction (XRD) **(**Figure 2.2b). In XRD, α-chitin and β-chitin are be distinguished by the different positions of the diffraction peak corresponding to the (020) inter-sheet distance. For β-chitin, this peak was at 7˚ while for α-chitin this peak was shifted to higher angles of 9˚- 9.5˚ corresponding to smaller (020) inter-sheet distance due to the increased degree

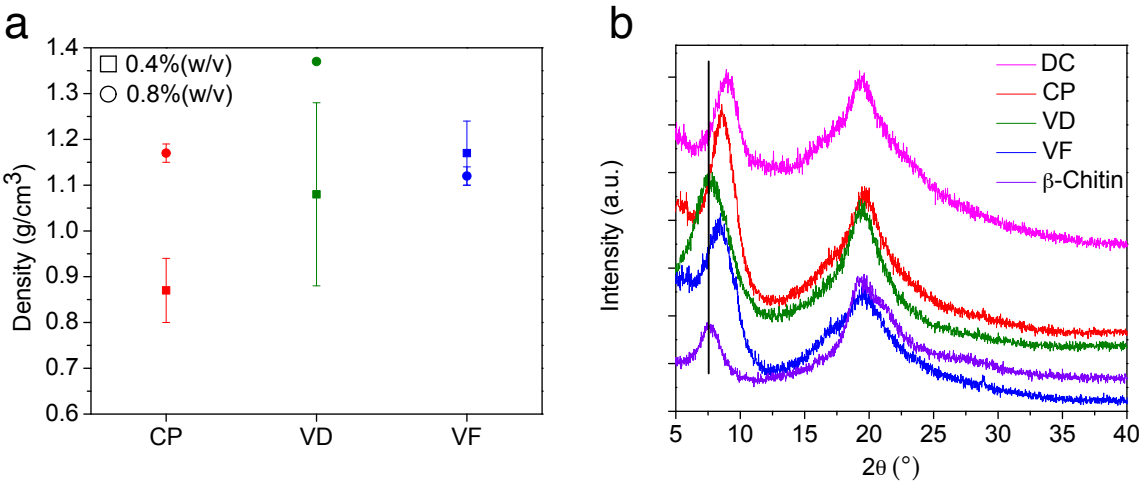

Figure 2.2. (a) Plot of density versus fabrication method and chitin/HFIP solution concentration. (b) XRD spectra of chitin films prepared by CP, VD, and VF in comparison with the as received chitin powder and DC.

of hydrogen bonding between the chitin molecules. We have previously observed that in DC the β-chitin/HFIP solution self-assembles into nanofibers that are α-chitin. Here, I observed that the amount of α-chitin in the films varies with processing method. For the chitin films prepared by VF the (020) peak was at 8˚, which indicates that the formed film is a mixture of α- and β-chitin. For CP, a higher degree of α-chitin was present with the (020) peak at 8.5˚. These results suggest that a slower drying time corresponds to higher degree of transformation into α-chitin. This is likely due to the chitin chains having more time to rearrange in the lower energy α conformation. In order to investigate the macroscale mechanical properties of these chitin films, I performed tensile testing.

2.4 Mechanical Properties Evaluation

The stress-strain curves showed relatively consistent data for films fabricated by CP, VD, and VF for the two concentrations, 0.4% (w/v) (Figure 2.3a) and 0.8%(w/v) (Figure 2.3b). For the films fabricated by CP, VD, VF from 0.4%(w/v) chitin/HFIP, the elastic moduli were 1.3 GPa, 1.5 GPa, and 2 GPa, respectively (Figure 2.3c). These results were consistent with the denser film having higher elastic modulus (Figure 2.2a). The elastic moduli for the on average denser films produced by 0.8% (w/v) chitin solutions were higher than the counterparts prepared with the 0.4% (w/v) solutions (Figure 2.3c). The VF method produced films from both concentrations with the same elastic modulus of 2.0 GPa. Tensile strength (σ_{ts}) also increased with denser films from 105.5 MPa (CP), 54.6 MPa (VD), and 129.3 MPa (VF) for 0.4%(w/v) solutions to 146.6 MPa (CP), 111.3 MPa (VD), 123.1 MPa (VF) for 0.8%(w/v) (Figure 2.3d).

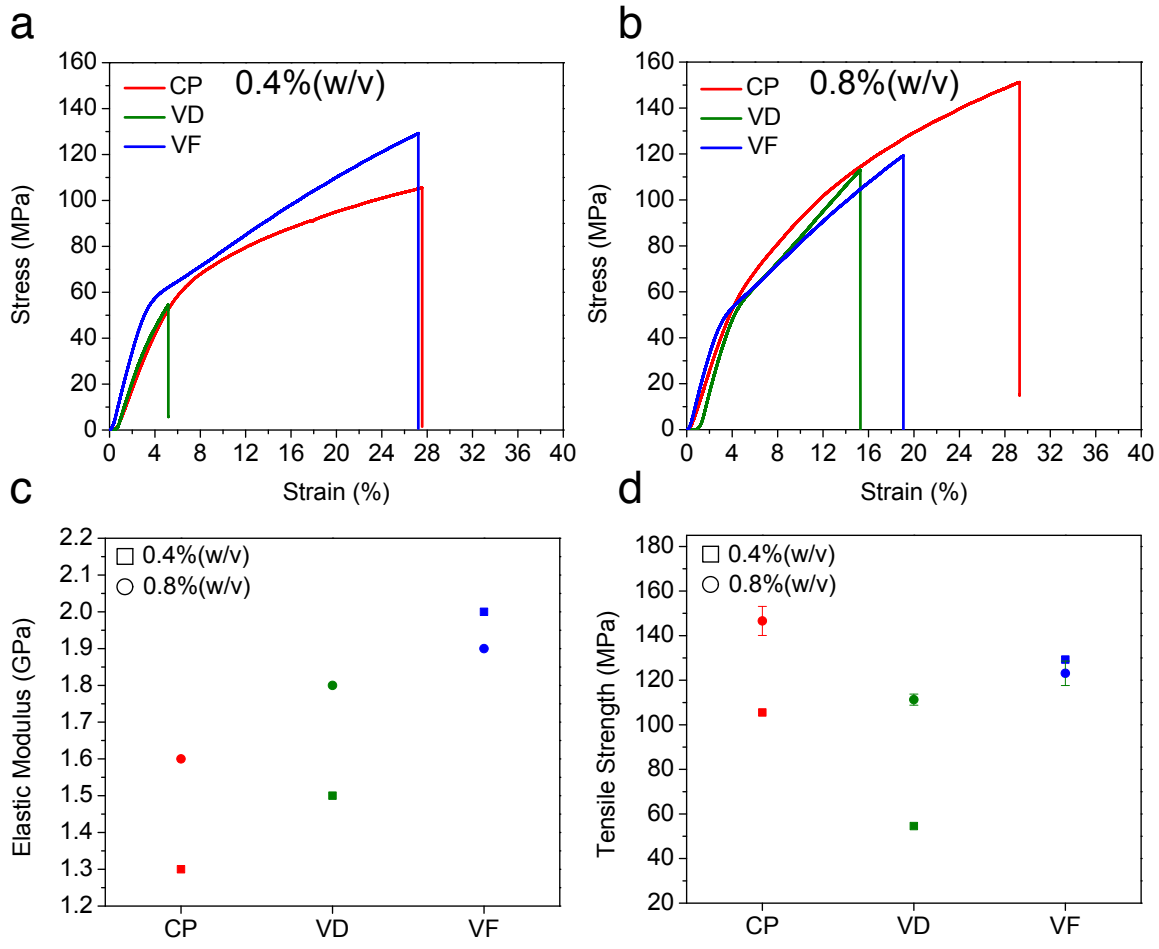

Figure 2.3. Mechanical properties of chitin films prepared by three methods, cold-press, vacuum filtration, and vacuum desiccator. (a) Stress-strain curves of films prepared by different methods for 0.4 wt% solution (b) Stress-strain curves of films prepared by different methods for 0.8 wt% solution. (c) Elastic modulus as a function of fabrication method and solution concentration. (d) Tensile strength versus fabrication method and solution concentration.

Films produced from CP had highest tensile strength regardless of a lower density compared to the films from VD and VF. The lower tensile strength for VD and VF films can be attributed to a lower film quality and existence of flaws and notches according to Weibull statistics.[29] The tensile strength for VF is the same for both concentrations.

For, single fiber network components such electrospun polymers [30, 31] and collagen fibers [32, 33], the elastic modulus of single fibers, E_f, can be extrapolated from the bulk film modulus, E, by the first order approximation and relative density ρ/ρ_f according to: [34-36]

$$E_f = 1.5 \times E \times \left(1 + \frac{\rho}{\rho_f}\right) \times \left(\frac{\rho}{\rho_f}\right)^{-2} \qquad \text{Equation 1}$$

Where ρ is the density of the nanofiber film and ρ_f is the density of the solid fiber material, for chitin 1.425 g/cm^3. For, CP, VD, and VF the single fiber elastic modulus calculated from Equation 1 is the range of 5-7 GPa. This small range indicates, that all methods produce similar quality chitin nanofibers. As expected, the elastic modulus of individual fibers is higher that elastic modulus of the bulk films due to the bending of fibers in an intertwined network. [34]

Our collaborator, Prof. Graham Cross, in Trinity College of Dublin, used flat punch nanoindentation on drop cast chitin films in order to probe the stress-strain mechanics of nanometer thick chitin layers [37, 38] In brief, a punch of diameter *2a* is brought into conformal contact with a film of initial thickness h_0 and load *L* is applied, indenting to residual thickness *h* **(**Figure 2.4a). Chitin samples are prepared by dropcasting from 0.05 % solution onto clean, polished silicon substrates and the final film thickness is measured by SEM cross section. The stress-strain and corresponding load-displacement response of a 250 nm chitin layer demonstrate a quite characteristic viscoelastic behavior (contrary to the typical elastoplastic response of a thin polymer layer for example cf. polystyrene[38]) where the elastic response increases with increasing strain **(**Figure 2.4b). They also performed a load-unload cycle for multiple indentations spaced 10 um apart at loading rates of 0.4 and 0.04 mN s^{-1}. The viscoelastic response of the chitin nanofiber network showed dependency on loading rates in a way that smaller displacement is observed with the higher loading rate for constant amount of load **(**Figure 2.4b). In the stress-strain data, surface roughness and intrinsic inhomogeneity are likely responsible for the small scatter in the data, but as expected the repeatability of the average response of the material under the punch diameter is reasonably good.

Axisymmetric flat punch nanoindentation of viscoelastic layers and extraction of material parameters, particularly through creep experiments, has been studied both experimentally and theoretically. [39, 40] The typical time-dependent viscoelastic relationship between stress (σ) and strain (ε) given by:

$$\sigma = E\varepsilon(t) + \eta\frac{d\varepsilon}{dt}, \qquad \text{Equation 2}$$

where E is Young's elastic modulus and η is an effective viscosity. Chitin responds with a strain-dependent response indicative of that described by Equation 2 (Figure 2.4b), and when

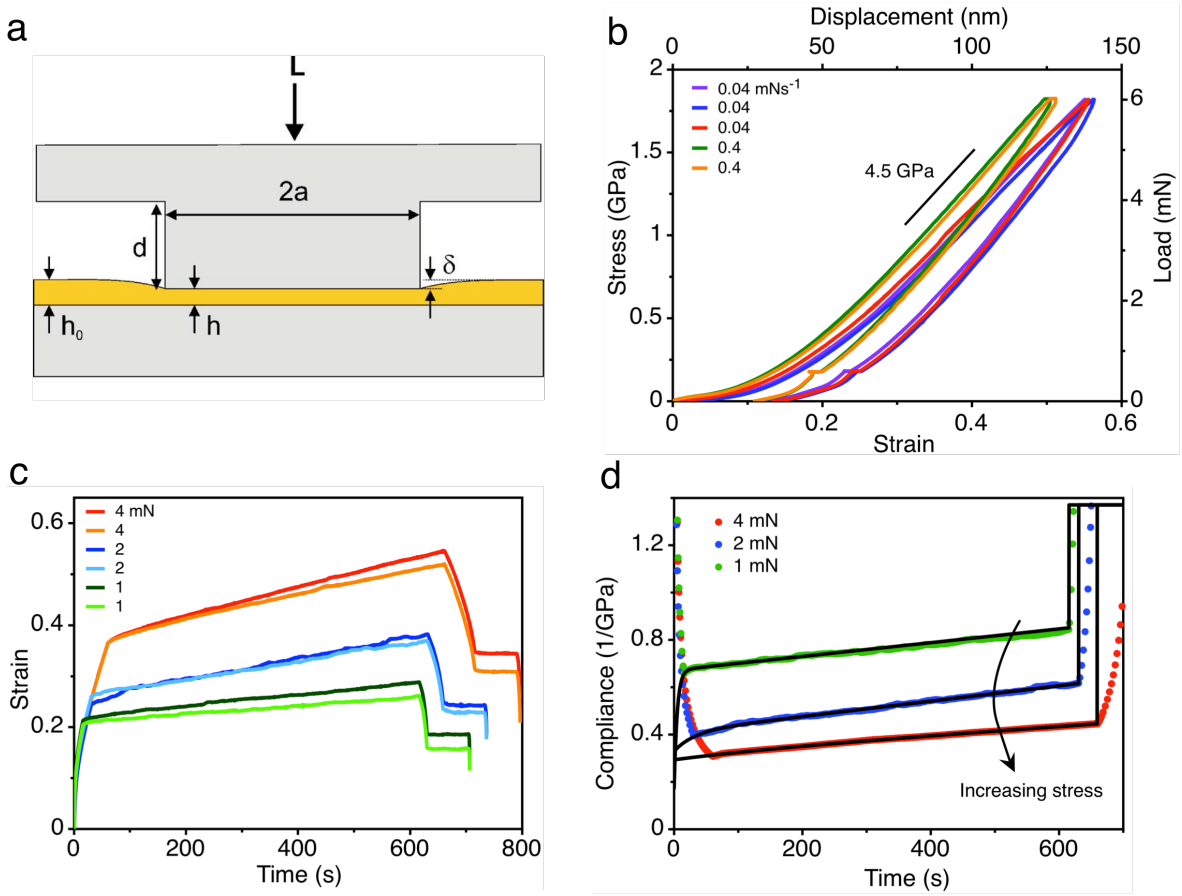

Figure 2.4. (a) Schematic of flat punch nanoindentation experiment in thin films. (b) Stress-strain (and corresponding load-displacement) response of 250 nm chitin layer for two different loading rates. (c) Creep response at three loading states. (d) Creep data represented as compliance against time, and corresponding non-linear fits to Equation 3.

approaching 40% compressive strain the chitin layer responds with an effective modulus in the range of 4-5 GPa. The low strain modulus (ca. 2 GPa) is in good agreement with bulk tensile testing described earlier and the high strain modulus is in good agreement with the single nanofiber modulus calculated earlier. They observed no evidence catastrophic structural failure up to 1.8 GPa of compressive loading, and the residual plastic strain is below 15% after complete unloading.

To gather further insights in the mechanical properties of chitin nanofiber thin films, they performed creep experiments by loading to, and subsequently holding, a constant stress with time. A series of 600 s creep experiments (all at different locations) corresponding to a constant load of 1, 2 and 4 mN show the typical slow increase of strain with time corresponding to a creep process **(**Figure 2.4c). The spread in data seen at each load level is a result of slightly different initial strains and varying drift rate, usually decreasing with each subsequent indentation as the instrument stabilizes. We may consider a Kelvin-Voigt type model for viscoelastic materials, where the creep compliance *J=The* is given by:

$$J(t) = \frac{1}{G_0} + \frac{1}{G_d}\left[1 - \exp\left(\frac{-t}{\tau}\right)\right] + \frac{t}{\eta}, \qquad \text{Equation 3}$$

where G_0 and G_d are the instantaneous and dynamic moduli respectively, and τ is the characteristic Voigt relaxation time. Such a model considers the elastic response of the material as a single spring in parallel with a 'dashpot' representing the viscous response, and may well be an oversimplification, but we shall use it here as a starting point. In Figure 2.4c presented as compliance against time. They performed chi-squared minimized non-linear fits of equation (3) to this data, where free fitting parameters are G_0, G_d, τ, and η_{max}. The fits are of high quality with chi-squared less than one in all cases, shown by the solid lines in figure 8d. The parameters derived from the fits in all cases correspond to a dynamic compliance $1/G_d = 2\pm1\times10^{-4}$ GPa^{-1} and effective viscosity of $\eta a = 4\pm1\times10^{5}$ Pa s, a viscosity comparable to a high molecular weight polymer melt. These figures correspond a dynamic modulus of around G_d = 5 GPa and instantaneous modulus of ca. G_0 = 200 GPa, consistent with values discussed previously.

2.5 CONCLUSION

In conclusion, I have developed three new fabrication techniques to make flat and high quality chitin nanofiber films from the self-assembly of chitin nanofibers from a chitin/HFIP solution. These techniques provide control of nanofiber film density, network structure, and mechanical properties. This modification of microstructure and properties through processing provides us the ability to tune the density and the mechanical properties for specific applications. From mechanical testing we have derived the single chitin nanofiber elastic modulus to be in the range of 5-7 GPa, which is consistent with flat punch nanoindentaiton studies. This modification of microstructure and properties through processing provides us the ability to tune the density and the mechanical properties for specific applications. These applications include substrates for tissue engineering, materials for soft-contact lenses, and membrane filters for water purification.

2.6. MATERIALS AND METHODS

Materials: Chitin squid extract (Industrial Research Ltd-New Zealand) and hexafluoro-2-propanol (HFIP) (Oakwood Products, Inc.) were used as received.

Chitin Film Fabrication:

Cold-Press (CP): chitin gels were prepared by letting the chitin/HFIP in air for 3-5 days. Then, we put the gels in between the glass slides covered with hardened filter papers (Whatman ^{TM}) and press firmly with the help of two clips.

Vacuum Drying (VD): The solution of chitin/HFIP was drop cast onto a glass petri dish and let dry in a desiccator connected to the house vacuum. The film was ready after 2-3 days.

Vacuum-assisted Filtration (VF): In this method, the solution of chitin/HFIP was drop cast into a porcelain funnel covered the PDMS-coated filter paper. PDMS-coated filter paper was prepared by spin coating PDMS on the filter paper on the speed of 500 rpm for 5 seconds and then 5000 rpm for 1 minute. The resulting fresh PDMS-coated filter papers were dried in the over for 3 hours at 60°C. The porcelain funnel was connected to house vacuum and covered with a glass cover in order to minimize evaporation from the top surface of the chitin film. The drying time for this method was about 1 day.

Atomic Force Microscopy: A Veeco Multimode V (Nanoscope IV controller) and Veecoprobes Sb-doped Si cantilevers (ρ = 0.01-0.025 Ω.cm, k = 40 N/m, υ ~ 300 kHz) were used for atomic force microscopy (AFM).

X-Ray Diffraction: XRD spectra were obtained at room temperature with a wide-angle X-ray diffractometer (2θ=5-55°) (Bruker D8 Focus) with Cu K α radiation, operated at 40 KV and 40 MA.

Fourier Transform Infrared Spectroscopy: Fourier Transform Infrared (FTIR) spectra were recorded on free-standing substrates with a Bruker vector 33 FTIR spectrophotometer (4000 to 400 cm^{-1}, 4 cm^{-1} resolution).

Mechanical Testing: Stress vs. strain data of chitin films substrates were recorded with a Shimadzu AGS-X at a rate of 0.1 mm/min. For each fabrication method, 6 chitin strips (3 for each concentration) were cut from the original films for mechanical testing and they were examined carefully by optical microscope for any notches and microscopic cracks. The reported values are the average and the A bars represent the standard deviation for each measurement. Instrumented nanoindentation was performed using the load-controlled Dynamic Contact Module head of an MTS XP Nanoindenter, providing low noise and high resolution sensing (data are recorded for displacement steps of 0.15 nm). Nanoindentation testing was performed in an isolated environment at ambient conditions at a temperature of 20±1 °C and relative humidity of 40±10%. A diamond flat punch of 2050 nm in diameter, fabricated by focused ion beam milling, was brought into conformal contact with a 250 nm thick chitin layer on silicon. Samples were aligned by shallow indentation into an adjacent polymeric layer, scanning of the indent replica by AFM, and tilt correction of the sample from the vector offset of the punch face replica, as described in detail here.[38] Thermal drift was measured for each indentation (generally sub 0.1 nm/s) and linearly corrected for, along with load frame stiffness and sample mounting compliance.

Chapter 3. CHITIN NANOFIBER MICROPATTERNED FLEXIBLE SUBSTRATES FOR TISSUE ENGINEERING[23]

3.1 INTRODUCTION

The motivation for patterning the chitin films is the fact that engineered tissues require enhanced organization of cells and extracellular matrix (ECM) for proper function.[41-43] The cells reorganize according to the interaction with the ECM based on topography and mechanical properties such as matrix stiffness, elasticity, and viscosity.[44] Alignment of ECM molecules and concentration gradients of immobilized growth factors also play a crucial role in cellular organization.[43] To promote cell organization, substrates with controlled micro- and nanopatterns have been developed as supports for cell growth, and to induce cellular elongation and orientation via contact guidance in engineered tissues.[45-51]

3.2 Chitin Micropatterned Substrates Fabrication and Characterization

For this work, I prepared the chitin micropatterned substrates with replica molding of a "chitin nanofiber ink" (Figure 3.1). To create the desired substrates, an appropriate amount of chitin nanofiber ink was drop cast on the top of the mold and allowed to dry overnight in ambient conditions. In this work, I used PDMS replica of different gratings as molds to create the substrates. I chose micropatterns with 3.2 μm spacing (G1) and 12.2 μm spacing (G2) to evaluate the effects of groove spacing on cell alignment, G1 being smaller than the average cell diameter, and G2 being slightly larger than the average cell diameter. Supported chitin micropatterned substrates were obtained by placing a glass slide on the top of the solution during drying (Figure 3.1a). This simple strategy afforded the attachment of chitin nanofiber substrates to an arbitrary

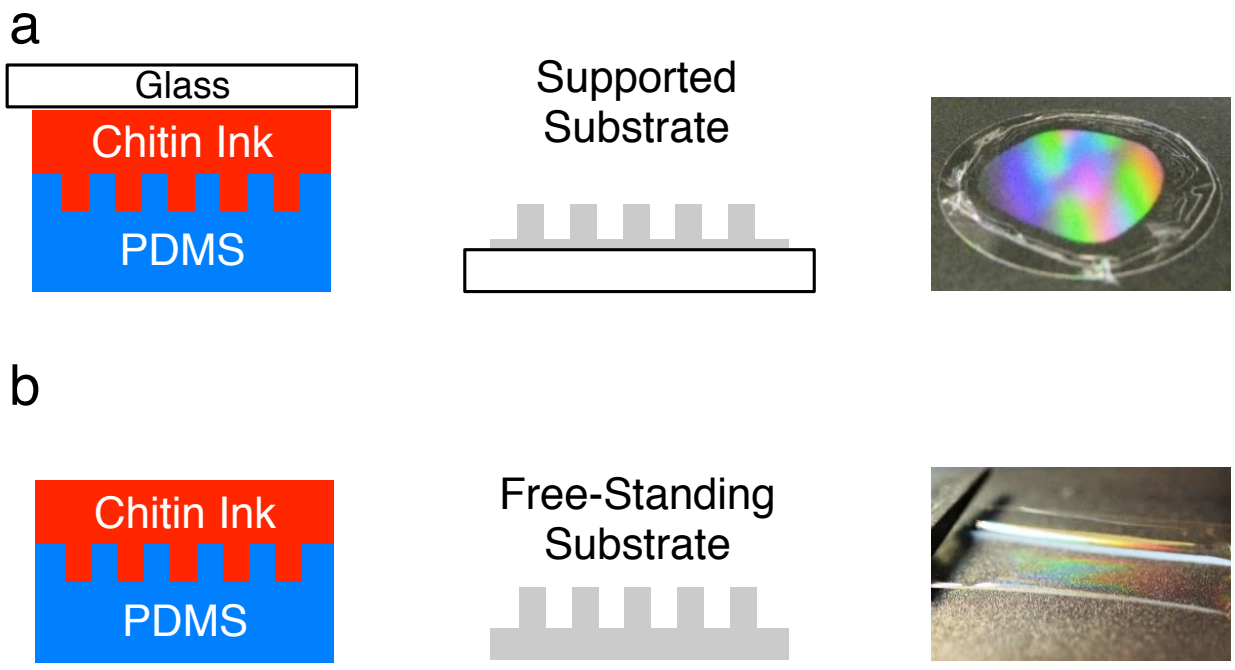

Figure 3.1. Chitin nanofiber-based micropatterned substrate fabrication process. Chitin/HFIP solution (0.1% (w/v)) was poured on the top of the (a) mold covered with a glass slide to create a supported substrate after drying overnight and its optical image with diffraction pattern on it (b) thicker films were obtained from more concentrated solutions (0.2% (w/v)) to create free-standing substrates. The optical image demonstrated the diffraction pattern on the free-standing chitin film.

support without requiring additional adhesive, which may be toxic for the cells. Free-standing substrates were typically thicker than the supported substrate and were peeled off directly from the mold (Figure 3.1b). The free-standing substrates were robust and could be easily lifted out from the molds with a pair of lab-tweezers. Both supported and free-standing were easy to handle and stable in cell culture media for extended periods of time. The microfabricated substrates prepared in this fashion exhibited the desired microstructure, which is inferred from the diffraction patterns in the optical images (Figure 3.1a and b) and AFM micrographs (Figure 3.2a and b). Micropatterned substrates G1 and G2 closely replicated the spacing and height of the original gratings (Figure 3.2c). As previously reported, chitin nanofiber random morphology was maintained intact in the micropatterns with the replica molding process (Figure 3.2d).[52] This replica molding process was low cost, easy to use, high throughput, and did not require expensive clean room equipment. With this simple solution processing micropatterned supported and free standing substrates were created in one step for further experiments.

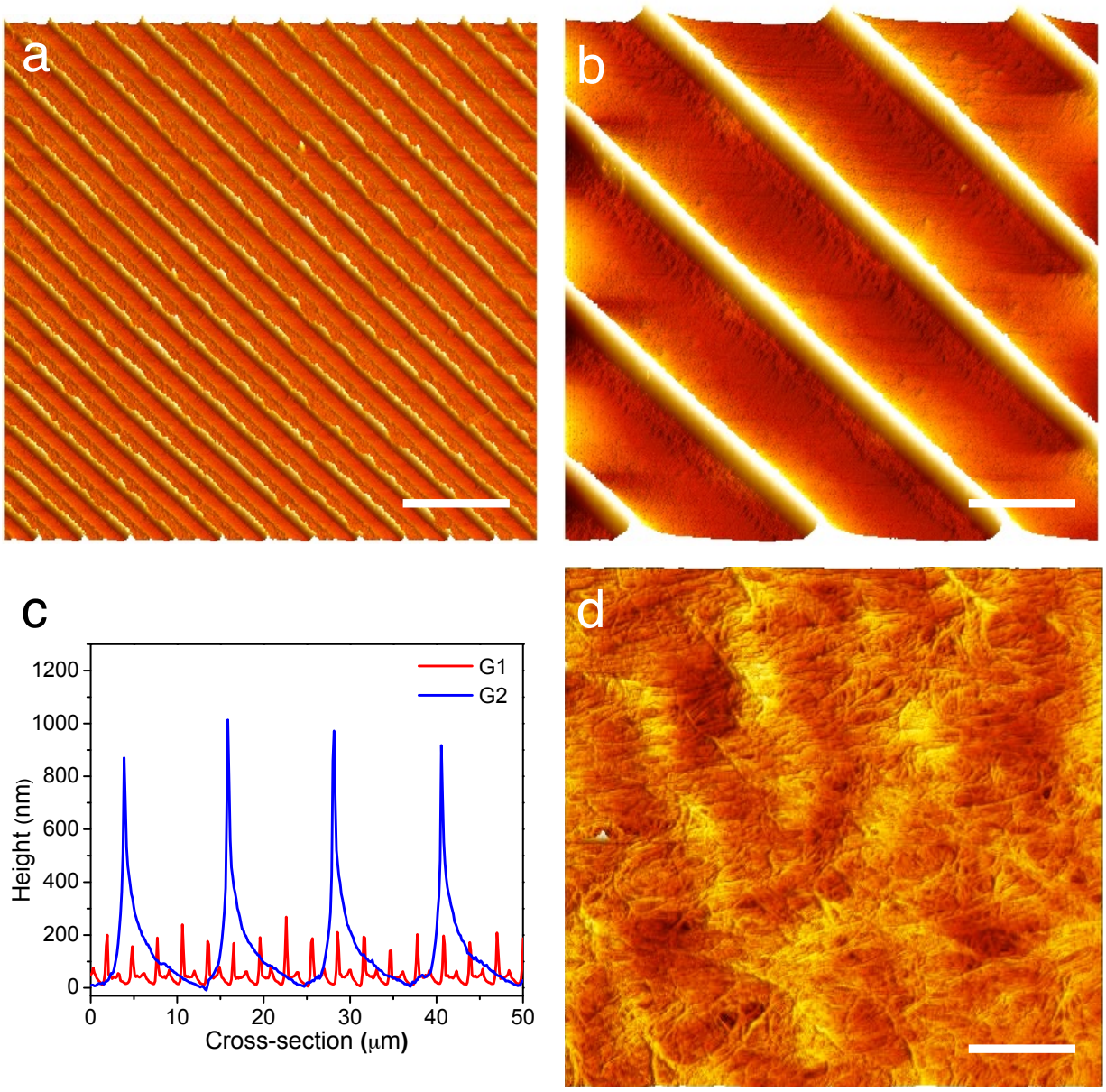

Figure 3.2. AFM imaging of supported chitin substrates (a, b) AFM height images of chitin substrates G1 and G2 respectively (Scale bar: 10 μm), (c) Cross-sectional height profiles of (a) and (b). G1 pitch= 3.0 ± 0.09 μ , height= 193.4 ± 30.4 nm and G2 pitch = 12.2 ± 0.2 μm and height 943.3 ± 62.6, (d) Zoom in of (b) showing chitin nanofiber morphology (scale bar = 200nm).

3.3 Fibroblast Cell Culture Analysis on Chitin Micropatterned Substrates

To employ the micropatterned nanofiber substrates for tissue engineering, NIH-3T3 fibroblast cells were seeded on the substrates with different size of groove and their behavior was subsequently investigated. This work has been done with collaboration with Prof. Khademhosseini lab at Harvard University. We chose fibroblasts for proof-of-concept because the organization of fibroblasts within the ECM of native myocardial tissue is critical to cell alignment, which influences the electrical and mechanical properties of the heart.[53] Fibroblast cell attachment on the as-prepared chitin substrates was low, as previously observed for neuronal cells, possibly due to the lack of reactive species and positive charges on the chitin surface.[22] To improve cell attachment, the chitin substrates were partially deacetylated and coated with a thin layer of fibronectin (FN). FN is an ECM protein and plays a major role in cell adhesion, growth, migration, and differentiation.[54] This deacetylation process of the chitin nanofibers allowed fine-tuning the chemistry of the substrates. The degree of deacetylation was measured as 30%. However, 30% deacetylation did not significantly affect the quality of the micropatterns. To evaluate the chitin substrates for tissue engineering, we cultured NIH-3T3 cells on the micropatterned and control chitin substrates and measured cell attachment, alignment, and proliferation. On the chitin micropatterned substrates, G1 and G2 (Figure 3.3a and b) cells with a spindle-like morphology aligned their cytoskeletal structure along the major axis of the micropatterned features (contact guidance). In contrast, the cells grown on the control chitin substrates did not have any preferred orientation (Figure 3.3c). We further quantified cells nuclei alignment on G1 and G2 micropatterns after 5 days of cell culture (Figure 3.3d, e, and f). In G1 and G2, a larger proportion of the cells aligned within the 0-10° preferred angle as opposed to control substrate (Figure 3.3f). The degree of cells nuclei alignment on G1 (~45%) and G2 (~55%) samples was significantly higher ($p<0.05$) than the degree of alignment for the control sample (15%) (Figure 3.3g). In addition, on G1 and G2, cell elongation increased with cell alignment. This increase indicated that the substrate topography affected cell morphology along with cellular alignment (Figure 3.3h). Cell attachment and proliferation was also evaluated with the direct cell counting method at days 1 and 5 of culture. NIH-3T3 fibroblast cells proliferated at day 5 of culture compared to day 1, indicating that the chitin substrates were non cytotoxic. In

addition, there was no significant difference in cell proliferation on different micropatterned samples (G1, G2) compared to the control substrate (Figure 3.3i).

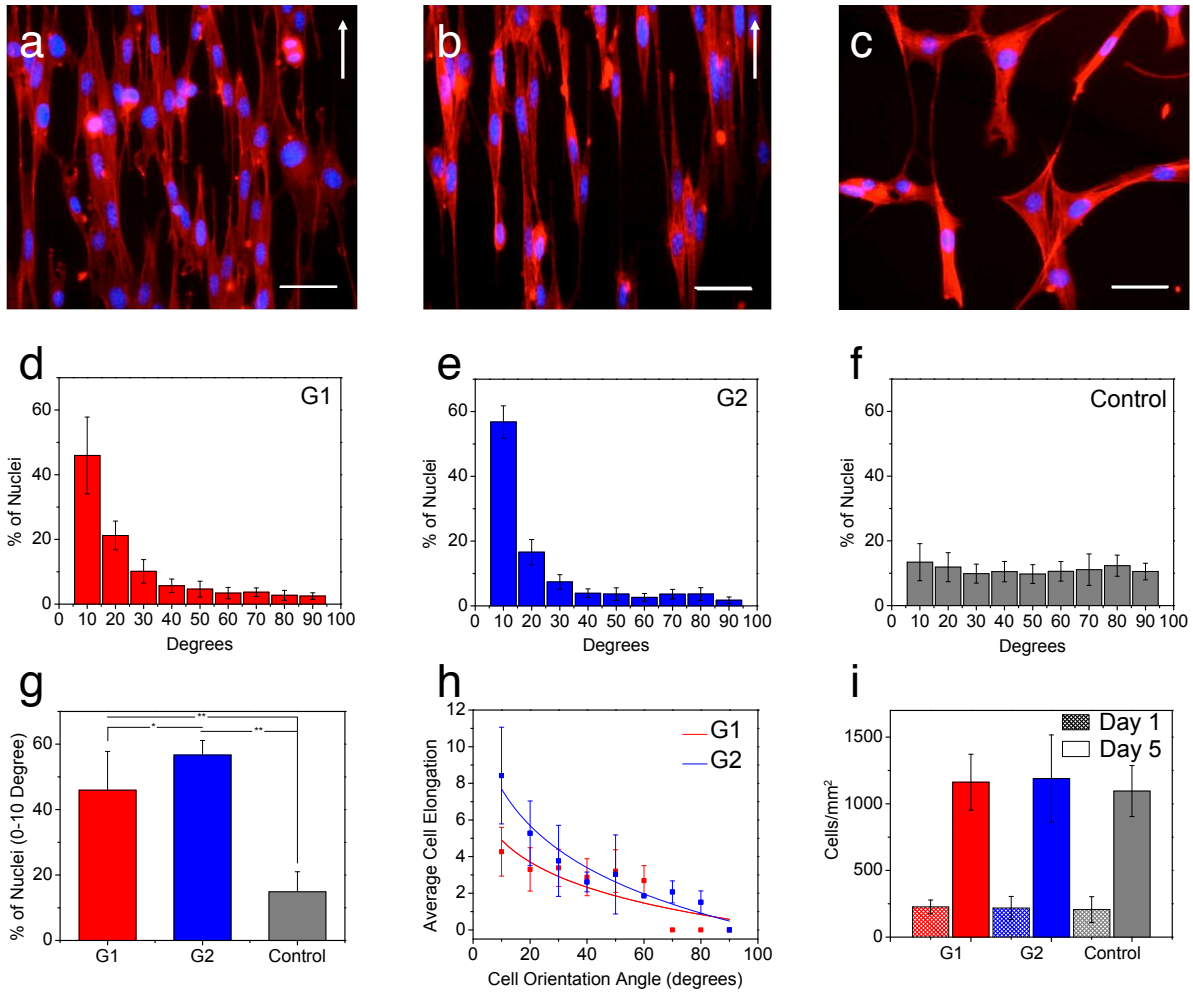

Figure 3.3. Fluorescence images of the actin cytoskeleton of the cells on (a) G1, (b), G2 substrates and (c) control sample after 5 days of culture (Scale bar 50 μm). The white arrow shows the longitudinal direction of the patterns. (d-f) Distribution of cells nuclei alignment angles on the patterned and control samples, (g) Percentage of cells that have orientation angles within 0-10 degree angle, (h) Cellular elongation function of cell orientation angle within the patterned substrates (i) Proliferation of the cells on the patterned and control substrates.

3.4 MECHANICAL PROPERTIES EVALUATION

The NIH-3T3-seeded free-standing films were sturdy and easily manipulated as well as flexible (Figure 3.4a) noting that the substrates absorb water and expand up to five fold their initial volume. Absorption of water is not surprising because the chitin nanofiber substrates themselves are hydrophilic and porous with a density of ~1 g/cm^3, which is lower than the density of chitin (1.44 g/cm^3). Water absorption and porosity are desirable properties to afford tunable optimal flow of nutrients to, and waste from the growing tissue. [41] To gather further insights on the mechanical properties of the substrates, I performed tensile test of the pristine chitin substrates, as well as the 30% deacetylated chitin nanofiber substrates before and after immersion in cell culture media for 1 and 5 days. The elastic modulus (*E*) of the pristine dry chitin substrates was 2.5 GPa with a tensile strength exceeding 100 MPa (Figure 3.4b). As expected from partial removal of the acetyl groups and corresponding lower degree of hydrogen bonding, the elastic modulus of the chitin substrates after deacetylation to 30% decreased to 926 MPa still retaining a tensile strength of 60 MPa (Figure 3.4b). These values for elastic modulus and tensile strength are significantly higher than the values previously reported for chitosan electrospun nanofibers (150 MPa).[55] Even after deacetylation to 30%, the self-assembled chitin nanofibers most likely still have a higher degree of crystallinity and stronger intramolecular hydrogen bonding from the remaining acetyl groups.[56] To investigate the mechanical properties of the substrates during cell culture, we measured substrates after immersion in PBS for 1 day immediately after removal from the solution while the substrates were still in the swollen state. The elastic modulus was 5 MPa with a tensile strength of 1 MPa (Figure 3.4c). Incorporation of water made the substrates more flexible and better suited for tissue engineering applications.[57, 58] In these applications, it is desirable for the substrate to have similar mechanical properties of the host tissue.[59-61] With these favorable properties, the cell-seeded chitin substrates were still mechanically robust but more flexible than the dry chitin and withstood bending and rolling to produce more complex 3D structures or transfer to the tissue of choice. These transparent, robust, ultra-thin, free-stranding chitin substrates covered with aligned fibroblasts with tunable and superior mechanical properties could make very a promising candidate to form 3D functional tissue and mimic the complex hierarchical of the ECM.

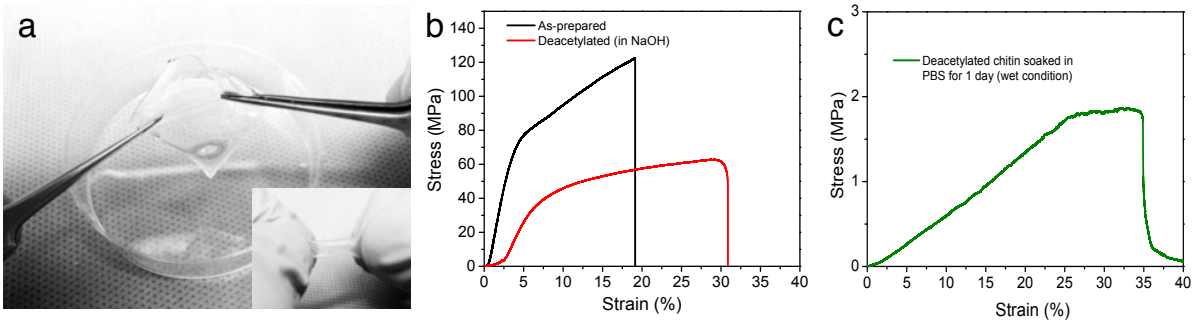

Figure 3.4. Cell seeded free-standing flexible chitin substrates, (a) Stretching and Rolling (insert) flexibility the free-standing micropatterned chitin substrates (G2) seeded with 3T3 fibroblast (b) Mechanical properties of micropatterned free standing chitin substrates before and after deacetylation to 30%, (c) mechanical properties of the 30% deacetylated chitin nanofiber substrates after immersion in PBS for 1 day (measured wet).

3.5 Conclusion

In this work, I have developed supported and free-standing micropatterned substrates made of self-assembled chitin nanofibers. These ultrathin micropatterned substrates are biodegradable, mechanically robust, yet flexible and easily manipulated. The substrates were seeded with NIH-3T3 cells that aligned along the major micropattern axis creating ultra-thin (<10 μm) and free-standing ordered cell sheets. These sheets are sturdy in cell culture media yet flexible and easily manipulated to create more complex tissue structures for regenerative medicine and tissue engineering applications.

3.6 Materials and Methods

Fabrication of Chitin Substrates: Substrates with micropatterns were fabricated using replica molding from a "chitin nanofiber ink" as previously described.[52] The chitin nanofiber ink was prepared by stirring appropriate amounts of β-chitin squid extract (Industrial Research Ltd-New Zealand) in hexafluoro-2-propanol (Oakwood Products, Inc.) for one week in ambient conditions. Two optical gratings (THORLABS) were used as masters: GE2550-3263 Echelle Grating with 3.16 μm spacing and 63˚ blaze angle (G1) and a GE 2550-0875 Echelle Grating, 12.66 μm, 75˚ blaze angle (G2). Replica molds were made with PDMS from SYLGRAD 184

(10% curing agent) and cured at 50˚C for 8 hours. The chitin nanofiber ink was drop cast onto the mold (50 µl) to create the micropatterned features. Alternatively, control substrates (no micropatterns) were prepared using a flat PDMS mold. Micropatterned and control substrate were supported on plasma-cleaned glass cover slips (Ted Pella, Inc.). For supported micropatterned and control substrate, a chitin solution of 0.1 % w/w was used. Free-standing chitin substrates were fabricated with a 0.2 % w/w chitin solution. Solutions of higher concentrations resulted in thicker films that were easier to handle. Both types of films were dried overnight in ambient and peeled off from the PDMS mold for further experiments.

Characterization of Chitin Substrates: A Veeco Multimode V (Nanoscope IV controller) and Veecoprobes Sb-doped Si cantilevers (ρ = 0.01-0.025 Ω.cm, k = 40 N/m, υ ~ 300 kHz) were used for atomic force microscopy (AFM). Fourier Transform Infrared (FTIR) spectra were recorded on free-standing substrates with a Bruker vector 33 FTIR spectrophotometer (4000 to 400 cm^{-1}, 4 cm^{-1} resolution). The degree of deacetylation (chitin vs. chitosan) was evaluated using the ratio of A_{1560}/A_{1030} according to a previously reported procedure.[22, 62] Stress *vs.* strain data of the free-standing substrates were recorded with a Shimadzu AGS-X. The substrates were tested dry before and after deacetylation as well as after immersion in Dulbecco's Phosphate Buffered Saline (DPBS) (GIBCO) for 1 and 5 days. Wet substrates were immersed in PBS for 1 day and tested immediately after removing from the solution.

Chemical modification of chitin substrate: Chitin substrates were partially deacetylated into and coated with fibronectin (FN) to improve cell attachment and proliferation. Deacetylation was performed with 5mM NaOH at 40°C for 1 hour. The substrates were then washed with distilled water three times and air-dried. FN (from bovine plasma, 0.1% sterile solution, Sigma-Aldrich) was coated on the substrate by incubating the chitin substrates in 200 µl of FN solution for two hours (T=37 °C). After incubation, the substrates were rinsed thoroughly in DPBS to remove the non-adsorbed and excessive aggregates of FN. The substrates were then dried in a desiccator overnight for further biological experiments.

Cell culture preparation: NIH/3T3 fibroblast cells were used in this work. The cells were maintained in T-75 flasks at 37 °C and 5 % CO_2 and cultured in Dulbecco's Modified Eagle Medium (DMEM) supplemented with 10% FBS and 1% penicillin-streptomycin. Prior to seeding cells on chitin substrates, the samples were rinsed in NIH/3T3 cell culture medium

twice. 80% confluent 3T3 cells were trypsinized, washed and suspended in fresh culture medium and subsequently the cell suspension was diluted with cell growth medium to reach the desired cell concentration. A cell suspension containing 1000 cells/500µl of medium was then added to each sample for further testing.

Cell proliferation and immunofluorescence for cytoskeletal organization: Cell attachment and proliferation on the micropatterned and control (without pattern) chitin substrates were evaluated with direct cell counting at days 0 and 5 of culture. Immunostaining assesses the actin cytoskeletal organization (F-actin) of the cells attached to different samples. The samples were washed for three times in DPBS and are fixed in 4% paraformaldehyde (PF) solution in DPBS for 20 min at room temperature. The substrates were then submerged in 0.1% Triton X-100 solution in DPBS for 30 minutes in order to permeabilize the cells' membrane and blocked in 1% Bovine Serum albumin (BSA) for 1 h. The actin cytoskeleton was stained using 1:40 dilution of Alexa Fluor-594 phalloidin (Invitrogen) in 1% BSA. Following immunostaining, the cell nuclei were stained with 1:1000 dilution of 4′,6-diamidino-2-phenyl indole dihydrochloride (DAPI) stain (Invitrogen) in DPBS for 5 min. Upon staining, the samples were imaged using an inverted fluorescence microscope (Nikon TE 2000-U, Nikon instruments Inc., USA) and the fluorescence images were analyzed using NIH image J software (version 1.4).

Quantification of cellular alignment and shape index: To quantify cellular alignment within micropatterned and control chitin substrates, fluorescence images were obtained at 5-6 different locations of each sample after 5 days of culture. The shape of each individual nucleus was first fitted with an ellipse and the normalized nuclei alignment were defined according to previously published procedure[63]. The normalized cellular alignment angles were finally grouped in 10 degree increments to compare the alignment of the nuclei on patterned and control substrates. Cell elongation within each sample was evaluated using fluorescence images of the cells cytoskeleton stained for F-actin filaments (5-6 regions). Cell elongation was determined as the ratio of cell length to cell width. The cell length was defined as its longest cord and the cell width was defined as the longest chord perpendicular to its length. The angle between the cells longest cord and the direction of the micropattern grating was defined as the cell orientation angle.

Chapter 4. A BIO-INSPIRED COMPOSITE FROM SOLUTION SELF-ASSEMBLY OF CHITIN NANOFIBERS IN A SILK FIBROIN MATRIX[64]

4.1 INTRODUCTION

Natural structural materials are made up of a biomineralized organic phase with exceptional fracture toughness based on chitin nanofibers often embedded in a silk-like protein matrix[17, 65]. This kind of structure leads to their outstanding mechanical properties coupled with low weight.[66] Despite these desirable properties, artificial bio-inspired composites based on chitin nanofibers have been difficult to produce again due to chitin's insolubility in most organic solvents.

4.2 CHITIN-SILK BIOCOMPOSITE FABRICATION

To create the chitin-silk biocomposite, solutions of squid pen β-chitin and *B. Mori* cocoon silk co-dissolved in HFIP were dried on a PDMS mold to yield homogeneous films (Figure 4.1).

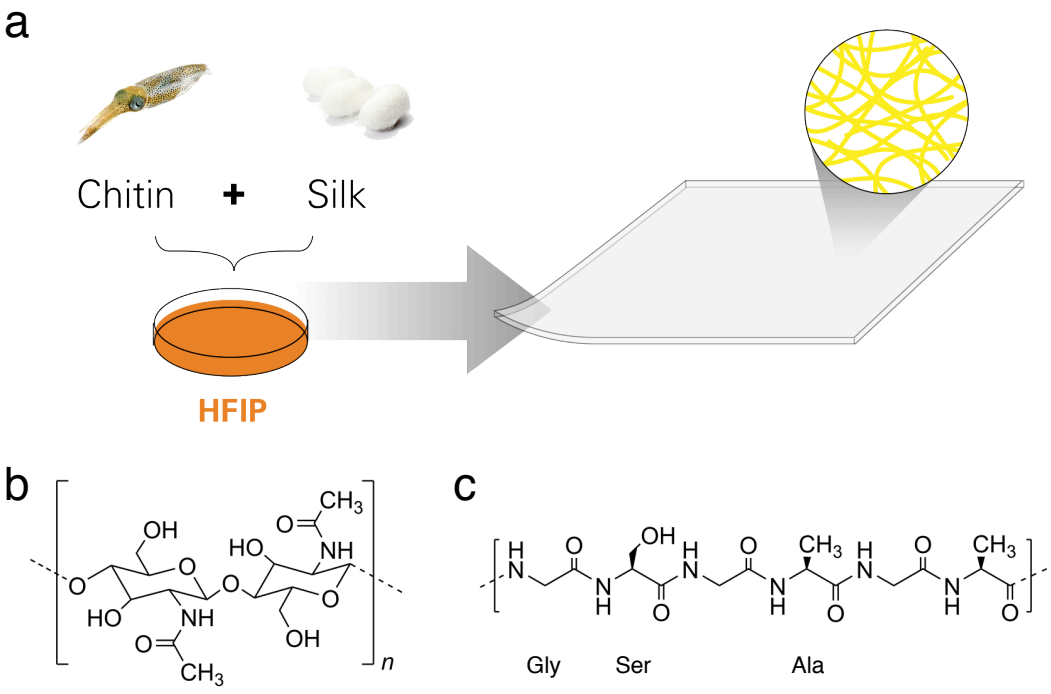

Figure 4.1. (a) Schematic illustration for the self-assembly process of the bio-inspired chitin nanofiber-silk hybrid biocomposites. Squid pen β-chitin and *B. Mori* cocoon silk are co-dissolved in hexafluoroisopropanol (HFIP) to yield clear hybrid solutions with different chitin:silk weight ratios. Upon drying, the solution forms a transparent biocomposite comprised of ultrafine (3 nm) chitin nanofibers self-assembled inside the silk fibroin matrix. (b) Molecular structure of β-chitin extracted from squid pen. (c) Primary chemical structure of silk fibroin extracted from *B. Mori* cocoon.

4.3 Chitin-Silk Biocomposite Film Characterizations

The pure chitin film was made of highly entangled ultrafine chitin nanofibers (Figure 4.2a). The chitin-silk biocomposite films were made of the ultrafine chitin nanofibers embedded in the silk fibroin matrix. The chitin nanofiber content of the biocomposite was easily tunable by varying the solution chitin/silk weight ratio in CS31, CS11, and CS13 (CSXY, where X:Y = chitin:silk weight ratio) (Figure 4.2b, c and d). This is a desirable feature that affords a simple strategy to fine-tune the biocomposite properties. In contrast, the surface structure of the silk film dried from the silk/HFIP solution was smooth and did not contain nanofibers, confirming that addition of chitin is essential to create the biocomposite nanostructure (Figure 4.2e). The self-assembly of

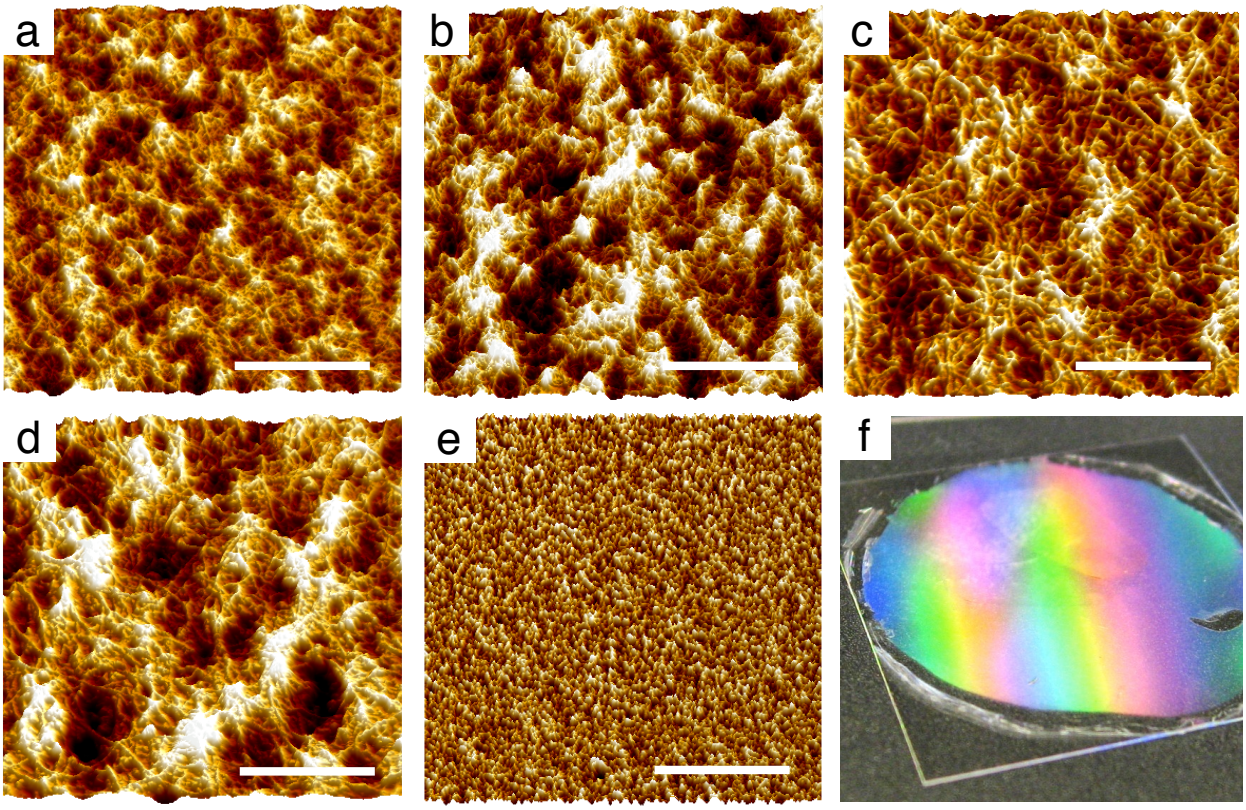

Figure 4.2. (a-e) Topographic AFM images obtained from films of chitin, CS31, CS 11, CS13, (CSXY, where X:Y = chitin:silk weight ratio), and silk, respectively. Scale bars 1μm. (f) Optical micrograph of transparent chitin nanofiber-silk hybrid formed into a diffraction grating from solution-based replica molding.

chitin nanofibers in the silk matrix was robust and occurred for a chitin/silk ratio as low as 1:30. The silk intercalate inside chitin fibers at first; at higher weigh ratios of silk to chitin, it also surround the entangled chitin nanofibers providing the silk matrix for the nanofibers.

The chitin-silk biocomposite films were transparent. The resulting dried films were likely solvent-free as HFIP is a poor hydrogen bond acceptor and does not form bonds with either chitin or silk.[26] The chitin-silk biocomposite assembled from solution was easily manipulated with soft-lithography strategies to manufacture optical elements such as diffraction gratings (Figure 4.2f). The chitin-silk biocomposite microstructure was further evaluated with XRD analysis (Figure 4.3).

As previously reported, α-chitin nanofibers self-assemble from the β-chitin/HFIP solution upon drying. The two characteristic XRD peaks were at 2θ=8.5° and 2θ=20.2° (Figure 4.3a, black) and corresponded to the reflection of the crystallographic planes (020) (*inter*-sheet) and (110) (*intra*-

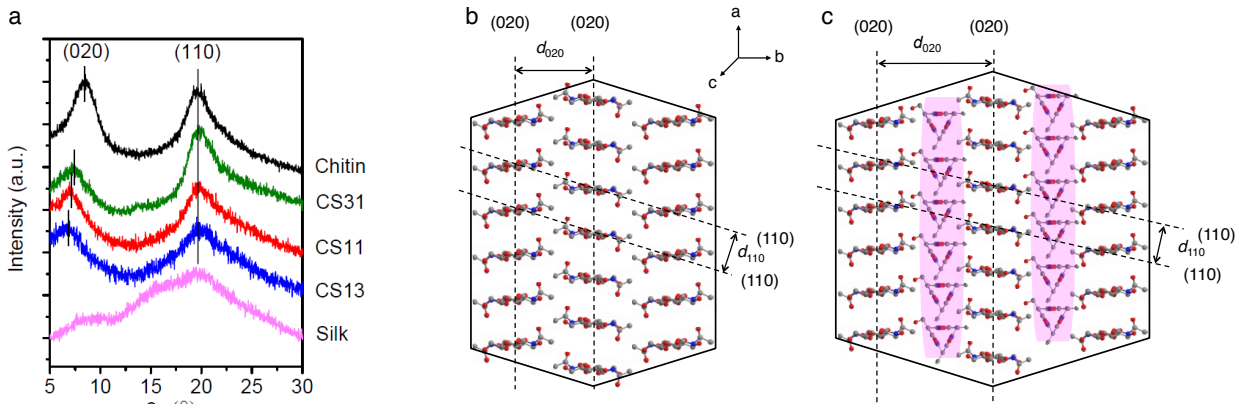

Figure 4.3. Crystal structure and micro-morphology of chitin-silk hybrid nanocomposites. (a) XRD patterns of chitin, CS31, CS11, CS13, and silk (b, c) Cross-sectional view (along c-axis) of a single chitin nanofiber and a chitin nanofiber within the chitin-silk biocomposite.

sheet) of the α-chitin orthorhombic crystalline structure (Figure 4.3b). The lattice parameters of α-chitin orthorhombic crystal system are as follows: a=0.474 nm, b=1.886 nm and c (fiber axis)=1.032 nm with the space group of $P2_12_12_1$. When chitin was co-assembled with silk, the (020) *inter*-sheet distance of the α-chitin nanofibers increased as indicated by the shift of the (020) XRD peak to smaller angles (Figure 4.3a, green, red, and blue). A reduced degree of crystallinity – (020) peak broadening – was also observed. I hypothesized that silk fibroin molecules intercalated in between the molecular sheets (020 planes) of the chitin nanofibers during the co-assembly process to maximize the degree of hydrogen bonding between the two biopolymers (Figure 4.3c). The interplanar spacing of (020) plane has been calculated for each chitin-silk composite according to Bragg's law ($n\lambda=2d_{hkl}\sin\theta$) (Table 1). The d values in the b direction increase by adding more amount of silk, which confirms the intercalation of silk molecules between chitin chains in the plane of (020). In the orthorhombic crystal system, the relationship between the d value and lattice parameters is defined with the following equation:

$$\frac{1}{d^2}=\frac{h^2}{a^2}+\frac{k^2}{b^2}+\frac{l^2}{c^2} \qquad \text{Equation 4}$$

The values of the lattice parameter, b, for chitin, and chitin-silk biocomposites can be calculated according to Equation 4 and values of d_{020} from Table 1. The results are shown in the Table 1. The lattice parameter, b, calculated for our developed α-chitin is 2.08 nm. This value increases 2.42 nm, 2.44 nm and 2.52 nm for CS31, CS11 and CS13. For the XRD peak at 2θ=20.2°, the values of interplanar spacing and corresponding lattice parameters for plane (110) were also calculated using the Bragg's law and Equation 4 and also considering already calculated b

values. The results are shown in Table 2. The lattice parameter, a, is showing the consistent value of 0.45 nm for chitin and all CS composites.

Table 1. Values of the 2θ degrees indexed for the *inter*-sheet (020) reflections from the XRD analyses and their corresponding interplanar spacings calculated by the Bragg's law.

Compound	Chitin	CS31	CS11	CS13
2θ (degrees)	8.5	7.31	7.25	6.98
Corresponding Plane (hkl)	(020)	(020)	(020)	(020)
The Wavelength of the X-ray Beam, λ (Å)	1.54			
Calculated Spacing, d_{020} (nm)	1.04	1.21 Δd=0.17 nm	1.22 Δd=0.18 nm	1.26 Δd=0.22 nm
Lattice Parameter, b (nm)	2.08	2.42	2.44	2.52

Table 2. Values of the 2θ degrees indexed for the *intra*-sheet (110) reflections from the XRD analyses, their corresponding interplanar spacings calculated by the Bragg's law and crystalline lattice parameters calculated by Equation 4.

Compound	Chitin	CS31	CS11	CS13
2θ (degrees)	20.2	20.2	20.2	20.2
Corresponding Plane (hkl)	(110)	(110)	(110)	(110)
The Wavelength of the X-ray Beam, λ (Å)	1.54			
Calculated Spacing, d_{110} (nm)	0.44			
Lattice Parameter, b (nm)	2.08	2.42	2.44	2.52
Lattice Parameter, a (nm)	0.45	0.45	0.45	0.45

The retention of chitin crystallinity and nanofiber formation of our biocomposites even from silk-rich solutions confirms the robustness of the chitin nanofiber self-assembly process in HFIP. This unique robustness of the intimate chitin-silk assembly in HFIP may be due to HFIP's strong volatility that facilitates revitalization of the hydrogen bonding upon drying, and also the capability of HFIP to stabilize the secondary structure of silk.

Fourier Transform Infrared Spectroscopy (FTIR) provides further insights in the molecular co-assembly process. For chitin, silk, CS31, CS11, CS13 the FTIR spectra contain signatures of chitin, silk, and both biopolymers, as expected (Figure 4.4). For pure chitin, the presence of α-chitin is confirmed by the Amide I (C=O stretching) split peaks at 1657 cm^{-1} and 1620 cm^{-1}. [67] These peaks are attributed to the hydrogen bonding of the C=O group of chitin to the -NH group of an adjacent chitin chain (1657 cm^{-1}) and with an -OH group on the same chitin chain (1620 cm^{-1}). The peak at 1635 cm^{-1}, usually associated with C=O binding only to –OH in β-chitin, in the α-chitin nanofibers may correspond to the C=O groups of the six chitin molecules on the surface of the nanofibers that do not fully participate in inter molecular hydrogen bonding. It must be noted, however, presence of some amounts of β-chitin in our samples cannot be excluded. By increasing the amount of silk fibroin in the sample, the frequency of the major chitin amide I band at 1657 cm^{-1} does not change in CS31, CS11, and CS13 (Figure 4.4b). However, there is an increase in intensity of the 1657 cm^{-1} peak, which is not expected from the simple sum of the chitin and silk spectra. This increase of the amide 1657 cm^{-1} peak may indicate additional hydrogen bonding between the C=O of chitin and the –NH group of silk (Figure 4.4c). Further indication of the chitin-silk hydrogen bonding is gathered from the shift of the amide II band (1557 cm^{-1}) and the reduction in intensity of the amide III band of chitin (1310 cm^{-1}) [68] with increased silk content in the biocomposite. Amide II and amide III in chitin correspond to the –NH bending and stretching modes mixed with the –CN stretching mode. This is particularly evident for the CS31 sample where the amide II band shift to higher frequencies and the amide III intensity reduction are prominent. The data for Amide III is the most convincing because the spectra of Amide III for chitin (1310 cm^{-1}) and silk (1335-1365 cm^{-1}) do not overlap. The Amide III in the chitin/silk biocomposite spectra is unequivocally assigned to the amide on the chitin molecule. From the silk spectra, the silk in the biocomposites is in the random coil confirmation (Silk I).[69] This FTIR data confirms a strong hydrogen bonding interaction between chitin and silk

in the biocomposite, although the exact structural nature of the bond will require further investigation.

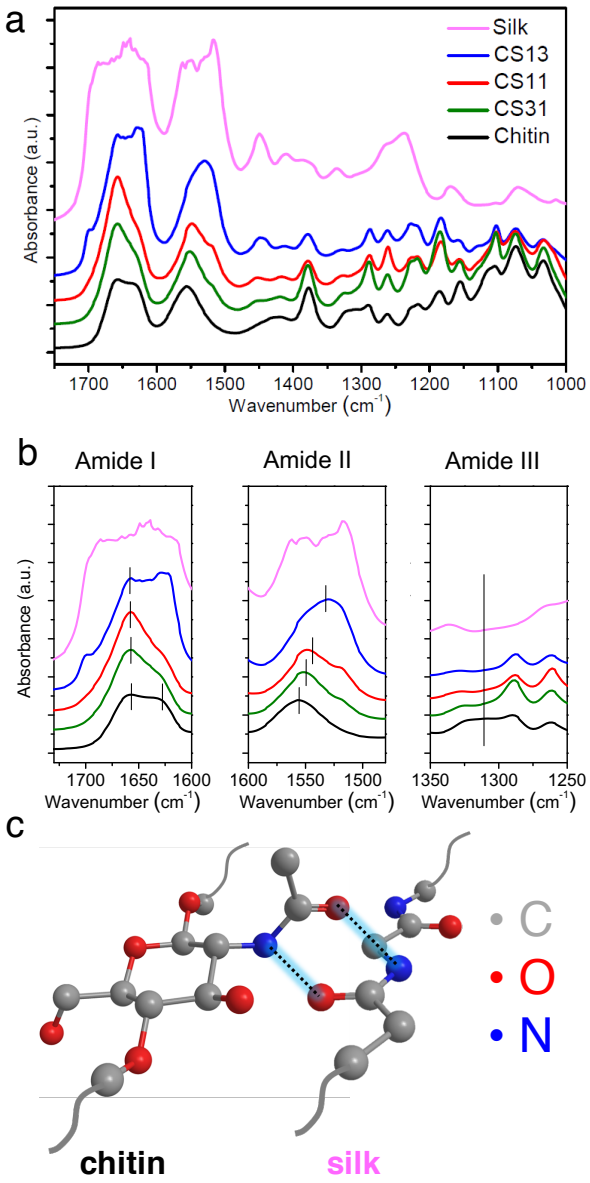

Figure 4.4. **(a)** FTIR spectra of chitin, CS31, CS11, CS13, and silk, (**b**) FTIR peaks for amide I (1657 cm^{-1} and 1620 cm^{-1}), II (1549 cm^{-1}) and III (1310 cm^{-1}) in chitin, CS31, CS11, CS13, and silk. In amide I, the 1657 cm^{-1} peak that corresponds to C=O, -NH interaction increases with silk content. For CS13, CS11, and CS31 there is a clear shift in the absorption maximum of amide II band, 1551 cm^{-1}, 1549 cm^{-1}, and 1534 cm^{-1}, respectively relative to that of pure chitin (1557 cm^{-1}). There is a strong reduction for amide III (1310 cm^{-1}) of chitin upon addition of silk. To note that Amide III of chitin and silk do not overlap. (**c**) Schematic illustration of the hypothesized hydrogen bonding motif between chitin and silk showing amide interaction within these molecules.

4.4 MECHANICAL PROPERTIES EVALUATION

The mechanical properties of the chitin-silk biocomposites confirmed the strong interaction between the chitin nanofiber phase and the silk matrix (Figure 4.5). On the basis of fiber composite theory,[70] I estimated the Young's modulus of our biocomposites based on the rule of mixtures: $E = KE_fV_f + E_mV_m$ (where, K = fiber efficiency parameter, E_f and E_m = Young's modulus of fiber and matrix respectively, V_f and V_m = volume fraction of fiber and matrix respectively). The Young's modulus of CS31 (E= 2.7 GPa) was higher than what is predicted by the rule of mixture (E = 0.9-2.0 GPa, when K = 0.4-1.0)[71] and even higher than that of pure chitin (E = 2.4 GPa). Amount of 25% silk content in CS31 seems to be the solubility limit of silk into chitin nanofibers. Upon addition of silk, the elastic modulus decreased in CS11 (E = 2.5 GPa) and CS13 (E = 2.2 GPa), but remained close to the elastic modulus of chitin, which proves that adding more silk over its solubility limit, 25%, does not help with increasing stiffness. This added silk surrounds the chitin nanofibers which might help with increasing strength and toughness in these composites. Also, the bonding of chitin and silk inside the nanofibers seem to play a major role in the stiffness of these composites. At small strain the elastic deformation of the hybrid composite is predominantly governed by the chitin nanofiber network despite the presence of intercalated silk. This behavior is consistent with the observation that a continuous nanofiber network exists even in the silk-rich CS13 (Figure 4.2d). The tensile strength of CS31 and CS11 was close to and exceeds 100 MPa, but did not surpass the tensile strength of the chitin film (113 MPa). The glass transition temperature (T_g) as a measure of binding between the phases in the biocomposites showed a trend consistent with the mechanical data (Figure 4.5b). T_g for CS31 was higher than T_g for the pure chitin film and the other biocomposite mixtures. Despite the high mechanical strength, the low T_g for the chitin-silk biocomposite afforded nano-embossing of the films for the easy production of nanoscale patterned samples (Figure 4.5c).

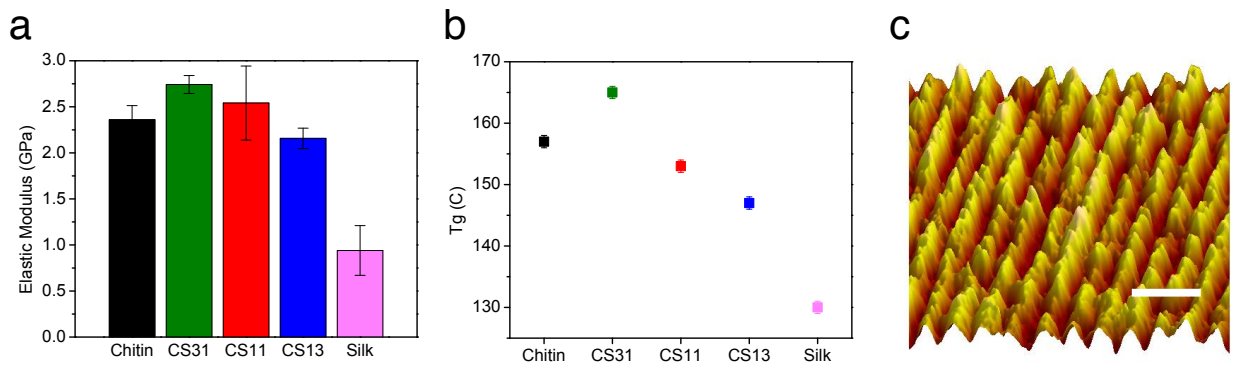

Figure 4.5. Mechanical properties of chitin-silk biocomposite films from tensile test and TMDSC (temperature-modulated differential scanning calorimetry) analysis. (a) Young's moduli obtained from slopes of linear region in engineering stress-strain curves of the biocomposites with different chitin/silk weight ratios. (b) Glass transition temperature derived from the TMDSC analysis of the chitin/silk biocomposites. (c) CS31 after nanoscale embossing at 170 °C with 150 psi of pressure (scale bar 2 μm).

4.5 Conclusion

In conclusion, I have demonstrated that a chitin nanofiber-silk biocomposite is easily co-assembled from homogeneous chitin-silk HFIP solutions. Chitin nanofibers self-assemble inside the silk matrix to yield a biocomposite that mimics the organic phase of the insect cuticle and the exoskeleton of crustacean, which are made of chitin nanofibers embedded in a silk-like protein matrix. This chitin-silk biocomposite is characterized by strong hydrogen bonding between the chitin nanofibers and the surrounding silk matrix. This interaction results in an increase in elastic modulus of the chitin-silk biocomposite respect to the elastic modulus of the separate components. The high transparency of the biocomposite coupled with the ease of solution processing and low $T_{g,}$ enable applications for optical components and nanostructured samples from solution based replica molding and nano-embossing. Chitin and silk are fully biocompatible and may find application in the biomedical field.

4.6 MATERIALS AND METHODS:

Materials: Chitin squid extract (Industrial Research Ltd-New Zealand) and hexafluoro-2-propanol (HFIP) (Oakwood Products, Inc.) are used as received.

Production of silk fibroin sponges: As previously described in the literature,[71] the purification of silk fibroin from Bombyx mori cocoons involves the boiling of the cocoons in a 0.02 M aqueous solution of sodium carbonate for 30 minutes to remove sericin. The remaining fibroin bundle is washed in deionized water and dried overnight at room temperature. The dried fibroin bundle is then dissolved in 9.3M aqueous solution of lithium bromide at 60°C for four hours. The resulting solution is dialyzed against DI water in dialysis cassettes (Slide-a-Lyzer, Pierce, MWCO 3.5K) to remove the lithium bromide salt. The remaining particulates are removed through centrifugation. This process enables the production of 6% w/v silk fibroin solution in water. Silk sponges are then obtained by freeze-drying the solution using a lyophilizer (LABCONCO®, USA) over 2days.

Preparation of Chitin-Silk Solutions: Appropriate amounts of β-chitin and silk fibroin sponges are dissolved in HFIP for two days under stirring at room temperature up to a total concentration of 0.2 w/v %. The chitin-silk solutions are CS31 (chitin/silk, 3 to 1 weight ratio), CS11 (1 to 1 weight ratio), and CS13 (1 to 3 weight ratio). Given the similar densities of chitin (1.44 g/cm^3) and silk (1.41 g/cm^3) the resulting biocomposites have the same v/v ratios as the solution wt/wt ratios. HFIP is a toxic solvent and particular care is required during handling. All the following procedures are performed in a fume hood. Composite films for further measurement and testing are prepared by pouring 50 ml of each solution into a rectangular-shaped polydimethylsiloxane (PDMS) mold. The molds are placed in a closed container to afford slow evaporation of the HFIP over a period of five days. Films obtained after shorter period of times are brittle due to increased number of defects and stress accumulated while drying.

Characterization: Tapping mode AFM is performed on a Veeco Multimode V with a Nanoscope IV controller. Veecoprobes Sb-doped Si cantilevers (ρ= 0.01-0.025 Ω-cm, k = 40 N/m, ν~ 300 kHz) are used. XRD spectra are obtained at room temperature with a wide-angle X-ray diffractometer (2θ = 5-55˚) (Bruker D8 Focus) with Cu K α radiation, operated at 40 kV and 40 mA. Fourier Transform Infrared (FTIR) spectra are recorded with a Bruker vector 33 FTIR spectrophotometer (4000 to 400 cm^{-1}, 4 cm^{-1} resolution). Stress vs. strain data are recorded three

rectangular samples for each material measuring 6 x 50 mm with thickness of approximately 20 μm. For silk, thickness is 70 μm. Before cutting the films for sample preparation, the films are hydrated using a vaporizer to remove residual stresses and avoid creating microcracks and defects during the cutting process. The samples are then dried overnight in ambient conditions. All tests are conducted based on the ASTM-D882-12 standard with a Shimadzu AGS-X (0.1 mm/min rate) equipped with a 100 N load cell and 50 N pneumatic grips. Temperature modulate differential scanning calorimetry (TMDSC) is used to characterize the glass transition temperature (Tg) of chitin, chitin-silk, and silk films. TMDSC measurements are performed using the protocol already reported[69] with a TA Instruments Q100, equipped with a refrigerated cooling system. Samples are heated at 2 °C/min from 30 °C to the beginning of the degradation temperature (250 °C for silk and 300 °C for pure chitin film), with a modulation period of 60 s and temperature amplitude of 0.318 °C. To determine the Tg, the reverse heath flow is plotted as function of temperature and the curve is fitted using Origin 8.5 and a Boltzmann exponential decay. The flex of the curve represents the glass transition temperature of the sample.

Imprinting: Imprinting of chitin-silk films is performed using a custom made embosser. A freestanding film was imprinted at 170 °C and at ~150 Psi for 30 s using a PDMS master.

Chapter 5. ULTRASTRONG AND FLEXIBLE HYBRID HYDROGELS BASED ON SOLUTION SELF-ASSEMBLY OF CHITIN NANOFIBERS IN A GELATIN METHACRYLOYL (GELMA) MATRIX

5.1 INTRODUCTION

Hydrogels are biological scaffolds with applications in tissue engineering and regenerative medicine.[72] Hydrogels are made from hydrophilic networks of polymers with porous structures that allow efficient for transport of oxygen and nutrients for optimal cell growth.[73] Hydrogels closely match the mechanical properties and flexibility of soft tissues for flawless organ integration. However, when hydrogels are too soft, their handling while maintaining tissue integrity becomes challenging.[74] To overcome this challenge, hydrogels are reinforced with more rigid components to create hybrids that are still soft but with improved mechanical robustness.[75] Here, we introduce the one pot self-assembly of new crosslinked gelatin methacryloyl (GelMA) hydrogels reinforced with chitin nanofibers (GMAC) (Figure 5.1). The chitin nanofiber reinforcement increases both stiffness and strain to failure of the hydrogels improving handling and integrity. The simple self-assembly process for these hydrogels is amenable to soft lithography strategies to create microstructures. Human Umbilical Vein Endothelial Cells (HUVECs) co-cultured with Human Mesenchymal Stem Cells (hMSCs) proliferate, and align on the micropatterned hydrogels and express vasculogenic markers indicating cellular differentiation and vascular network formation.

GelMA is a gelatin derivative that is synthesized by the direct reaction of gelatin with methacrylic anhydride (MA) (Figure 5.1b).[76] Gelatin is a hydrolytically degraded collagen, one of the most abundant components of the extracellular matrix (ECM).[73, 77] Photocrosslinking of GelMA using a water-soluble photoinitiator enhances stability of the water-soluble gelatin in tissue culture for applications in cardiac and vascular tissue engineering. GelMA is soft with elastic modulus of 3.3-110 KPa depending on degree of methacrylation and concentration of GelMA.[2, 78] As a result, reinforcement of GelMA is desirable for many applications. The elastic modulus of soft GelMA hydrogels increases from 10 KPa to 50 KPa upon reinforcement with aligned carbon nanotubes.[74] Also, adding silk fibroin to GelMA hydrogels increases its

compressive elastic modulus up to 80 KPa.[73] Following this exciting route, here we developed GelMA with self-assembled chitin nanofibers to make a fiber-reinforced hybrid hydrogels.

Chitin [poly (β-(1,4)-N-acetyl-D-glucosamine] (Figure 5.1c) is the second most abundant natural polysaccharide after cellulose.[4] Chitin occurs as ordered crystalline nanofibers and is the major structural component of cell walls in fungi and yeast, the exoskeleton of arthropods and mollusk shells.[20] Chitin is mechanically robust with elastic modulus of 2 GPa and ultimate tensile strength of 140 MPa comparable to aluminum.[79] Biomedical applications of chitin include sutures and wound dressings,[10] tissue engineering scaffolds,[4] microneedles for diagnostics,[80] and biocompatible electronic devices.[24] We have previously developed the self-assembly of 3 nm chitin nanofibers from solution[26, 79, 81] and demonstrated simple solution co-assembly of chitin nanofiber-silk biocomposites.[64] This solution process is amenable to facile soft-lithography strategies to create microstructures[82] for tissue engineering[22, 23] and biomedical devices. [21]

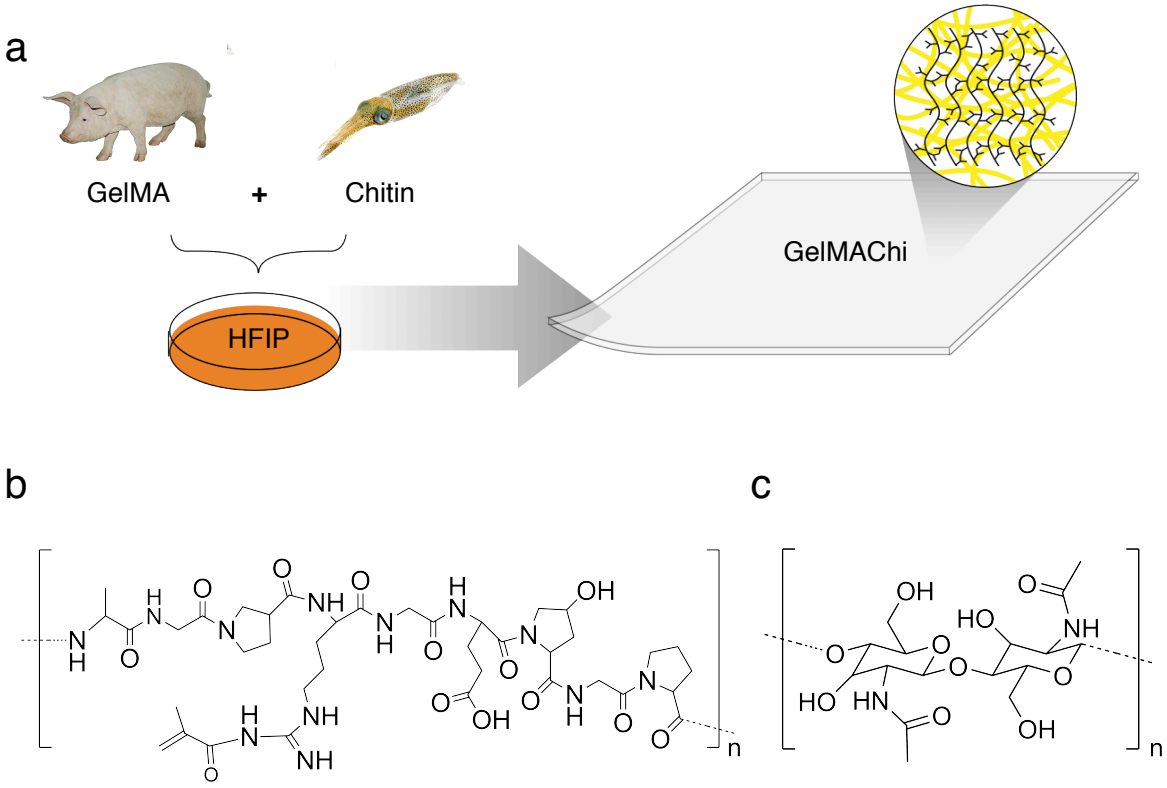

Figure 5.1. (a) Schematic illustration of the self-assembly process of chitin nanofibers-Gelatin methacryloyl (GMAC) films. Lyophilized porcine gelatin methacryloyl (GelMA) and squid pen β-chitin (Chi) are co-dissolved in hexafluoroisopropanol (HFIP) to yield clear solutions with different GelMA:chitin weight ratios. Upon drying, the solution forms transparent films comprised of ultrafine (3nm) chitin nanofibers self assembled in the matrix of UV crosslinked GelMA, (b) Molecular structure of GelMA, (c) Molecular structure of chitin.

5.2 CHITIN-GELMA HYDROGEL PROCESSING AND CHARACTERIZATION

Gelatin is water soluble and is not stable in aqueous environment.[73] To form chitin reinforced hybrid hydrogel, we first synthesize GelMA by functionalizing the primary amines in gelatin with methacryloyl groups according to previously published procedures (Figure 5.2a).[73] To create the GelMA-Chitin (GMAC) hydrogels, solutions of squid pen β-chitin and GelMA co-dissolved in HFIP are then dried on a polydimethylsiloxane (PDMS) mold to yield GMAC films (Figure 2b). The same process also yields films of gelatin and chitin nanofibers (GelChi) when pristine gelatin is used instead of GelMA. Exposure of GMAC to UV light (365 nm, 100W, 115V, UVP^{TM} Blak-Ray^{TM} B-100A UV Lamps) for 3 minutes in the presence of Irgacure 2959 as a photoinitiator crosslinks the methacryloyl groups in GelMA producing a covalently-bonded matrix intertwined with chitin nanofibers (Figure 5.2b). GMAC films are more stable in aqueous environment than GelChi films. In GelChi films, the entirety of the gelatin washes away after only one day in physiological conditions (Figure 5.3).

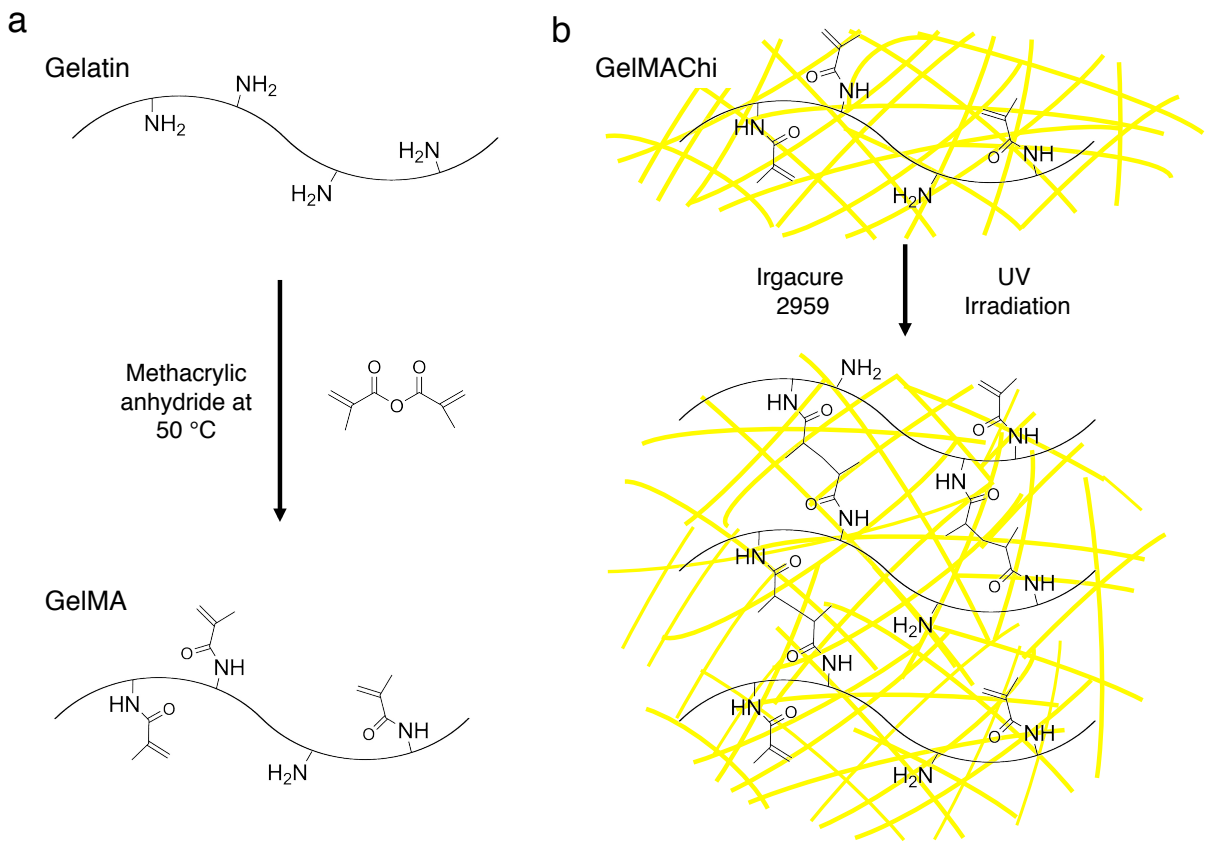

Figure 5.2. Synthesis of (a) gelatin methacryloyl (GelMA) through functionalizing gelatin's primary amine groups by mathacrylic anhydride (MA) at 50 °C, (b) Crosslinked GelMA-chitin (GMAC) films by exposure of dry GMAC films to UV irradiation in the presence of a photoinitiator (PI), Irgacure 2959, for 3 minutes. This process crosslinks the methacryloyl groups producing a stable covalently-bonded GelMA structure intertwined with chitin nanofibers.

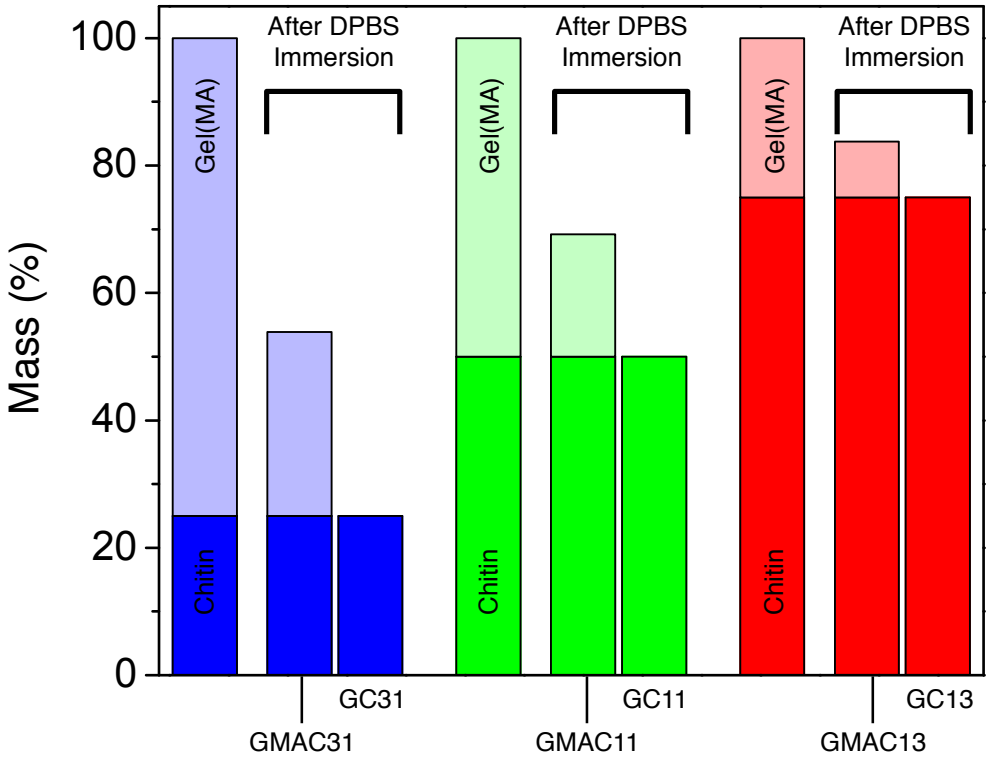

Figure 5.3. Values of mass percent showing stability of GelMA in comparison with gelatin in hybrid cross-linked GMAC (GMAC) hydrogels and gelatin-chitin (GC) hydrogels after immersion into DPBS for 24 hrs at 37 °C. Crosslinking GelMA will make it stable and less soluble in DPBS in comparison with fully soluble gelatin.

Chitin nanofibers self-assemble into the GelMA matrix and yield GMAC hybrid films with variable chitin nanofiber content (Figure 5.4). As prepared GelMA film is smooth (Figure 5.4a). Increasing the relative concentration of chitin and GelMA in GMAC31, GMAC11, GMAC13 (GMACXY, where X:Y = GelMA:chitin weight ratio) yields films with an increased fraction of chitin nanofibers as expected (Figure 3b, c, and d).[26] In GMAC31 (Figure 5.4b), the high amount of GelMA may result in the formation of GelMA agglomerates. In GMAC11 and GMAC13 (Figure 5.4c and d), the chitin nanofibers in the co-assembled hybrid hydrogel have the same entangled structure as the chitin nanofibers self-assembled from a chitin only-HFIP solution (Figure 5.4e) indicating the robustness of chitin nanofibers self-assembly in the matrix of GelMA. This microstructure control affords a simple strategy to fine-tune the mechanical properties of GMAC hydrogels. The GMAC films are solution processable and amenable to soft-lithography strategies that we have previously developed for chitin[23] and chitin-silk.[64] Micropatterns with the pitch of 12.15 μm and height of 450 nm are fabricated on GMAC13 using solution-based replica molding (Figure 5.4f).

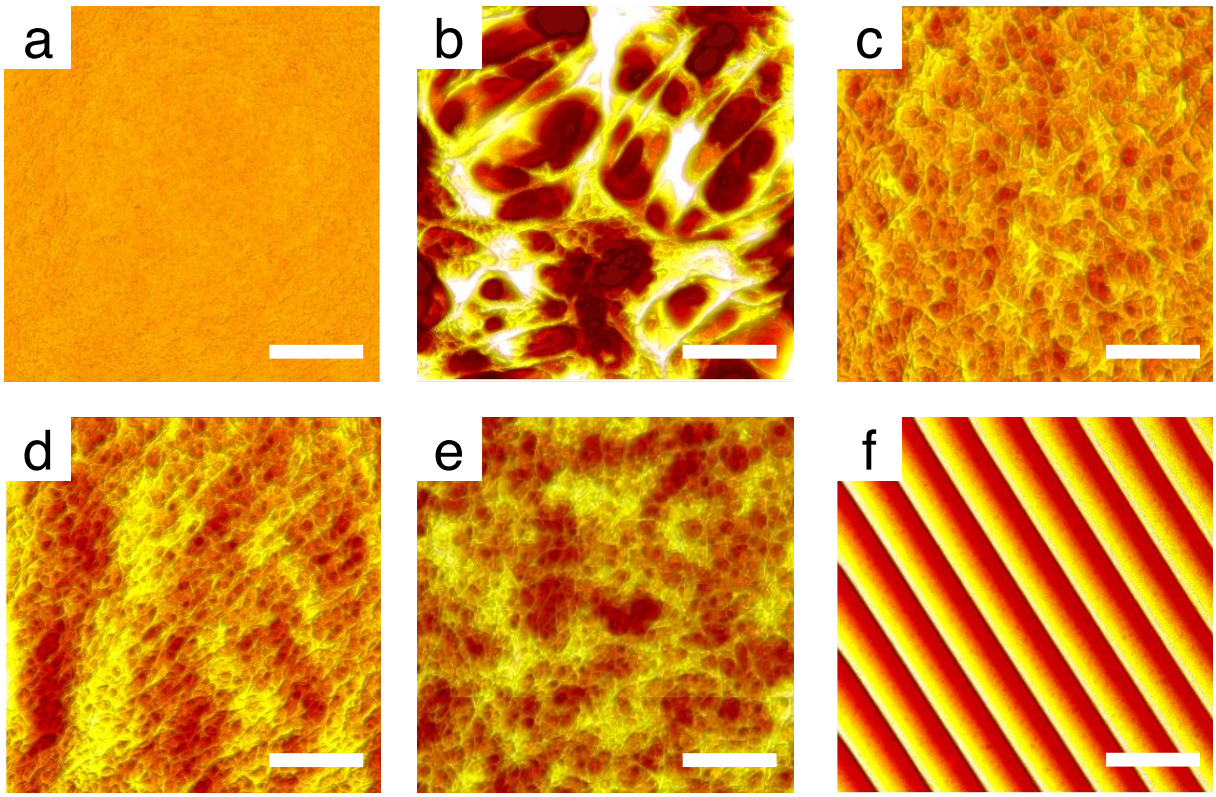

Figure 5.4. (a-e) Topographic atomic force microscope (AFM) images of GelMa, GMAC films with different GelMA:chitin weight ratios, and Chitin. GMACXY are GMAC films with XY = GelMA:Chitin weight ratio. (a) GelMA, (b) GMAC31, (c) GMAC11, (d) GMAC13, and (e) Chitin, respectively (scale bars are 500 nm). (f) Topographic AFM image of micro-patterned GMAC13 with a pitch of 12.15 μm and a height of 450 nm (scale bar is 20 μm).

5.3 MECHANICAL PROPERTIES EVALUATION

GMAC hydrogels are overall more robust than the GelMA counterparts without chitin nanofiber reinforcement (Figure 5.5). GelMA hydrogels have elastic modulus in the range of 3.3-110 kPa depending on the GelMA concentration and degree of methacrylation.[2] Chitin nanofibers in the matrix of GMAC hydrogels increase the elastic modulus significantly (from 3.3 KPa to 2.8 MPa for GMAC31 and to 4.6 MPa for GMAC11 and GMAC13) (Figure 4a). The increase in the elastic modulus for GMAC is due to physical reinforcement of soft matrix of GelMA with entangled chitin nanofibers. This increase in elastic modulus is more pronounced for GMAC13, which has higher content of chitin nanofibers. While we previously observed strong hydrogen bonding between chitin and silk, [64] GelMA and chitin do not show any substantial hydrogen bonding between the two molecules as indicated by Fourier Transform Infrared (FTIR) spectra (Figure 5.6).[64] This low degree of hydrogen bonding between GelMA and chitin might be due to a small number of available amine groups in the highly methacryloyl-modified (>80%) GelMA. These amine groups are required for hydrogen bonding with the C=O in chitin (Figure 5.2). It is likely that this reduced degree of hydrogen bonding in the GMAC composites causes a decreased elastic modulus from 633.6 MPa for chitin to 4.6 MPa for GMAC with only 10% GelMA (Figure 5.5a). It is conceivable that GelMA position itself between the chitin nanofibers, reducing the intrafiber hydrogen bonding, and acts as a lubricant to yield material with lower elastic modulus than what is expected from the rule of mixtures (Figure 5.5a). This lubrication effect affords, on the other hand, a very high strain to failure or extensibility of 224 % for GMAC hydrogels. This strain-to-failure is >100 % improvement with respect to GelMA hydrogels and > 200 % improvement with respect to chitin alone (Figure 5.5b-d). The GMAC11 and GMAC31 hydrogels also stretch 80 % more than chitin (Figure 5.5b). We select GMAC13 for cell culture because of its higher elastic modulus and superior extensibility (Figure 5.5c-d).

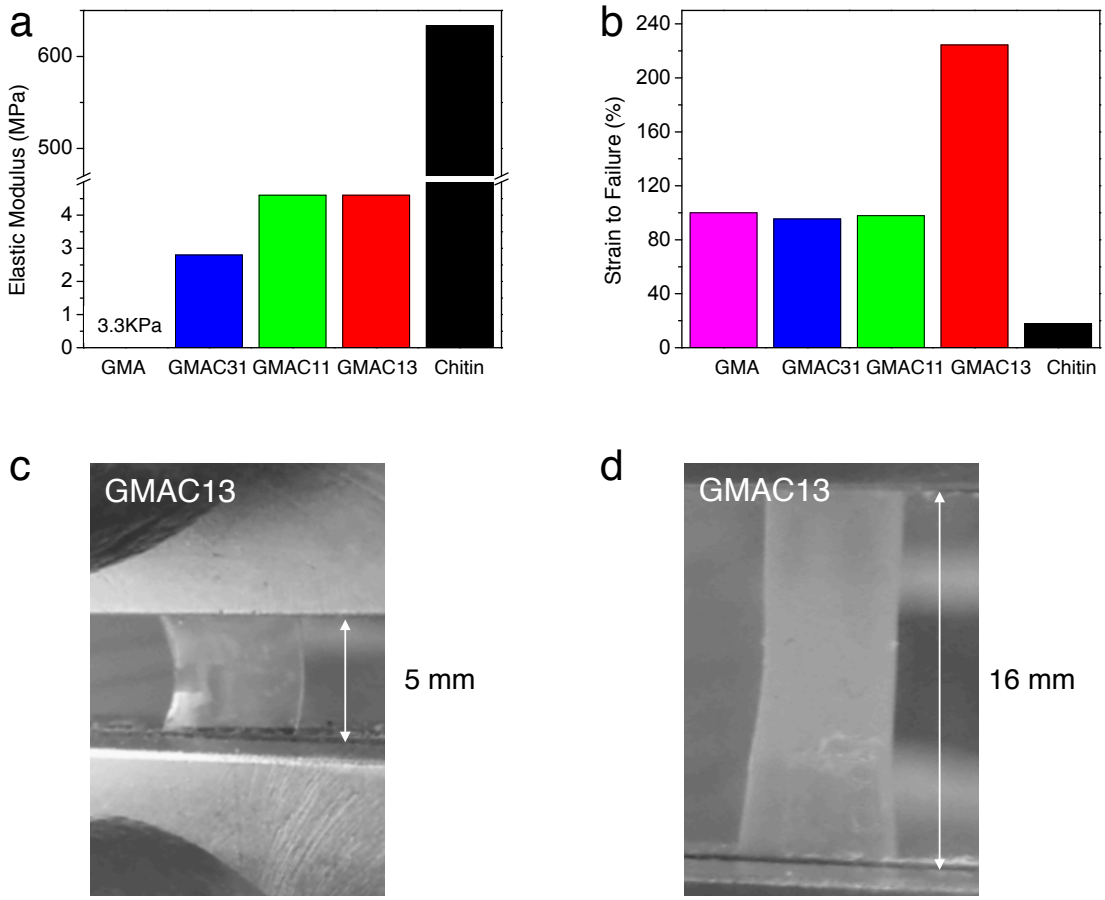

Figure 5.5. Mechanical properties of hybrid GMAC hydrogels from tensile test analysis, (a) Elastic moduli obtained from slopes of linear region in engineering stress-strain curves (Figure S4) of the hydrogels with different GelMA:chitin weight ratios. The elastic modulus for all GMAC hydrogels are higher than what has been reported for GelMA[2] and they are lower than chitin alone, (b) Values of engineering strain to failure for hybrid hydrogels with different GelMA:chitin weight ratios. GMAC13 is > 100% more extensible than GelMA[2] and > 200% more extensible than chitin alone, (c) Optical image of GMAC13 at the initial state before load application in mechanical tensile tester, (d) Optical image of GMAC13 showing 224% extensibility under tensile load, showing final length of 16 mm.

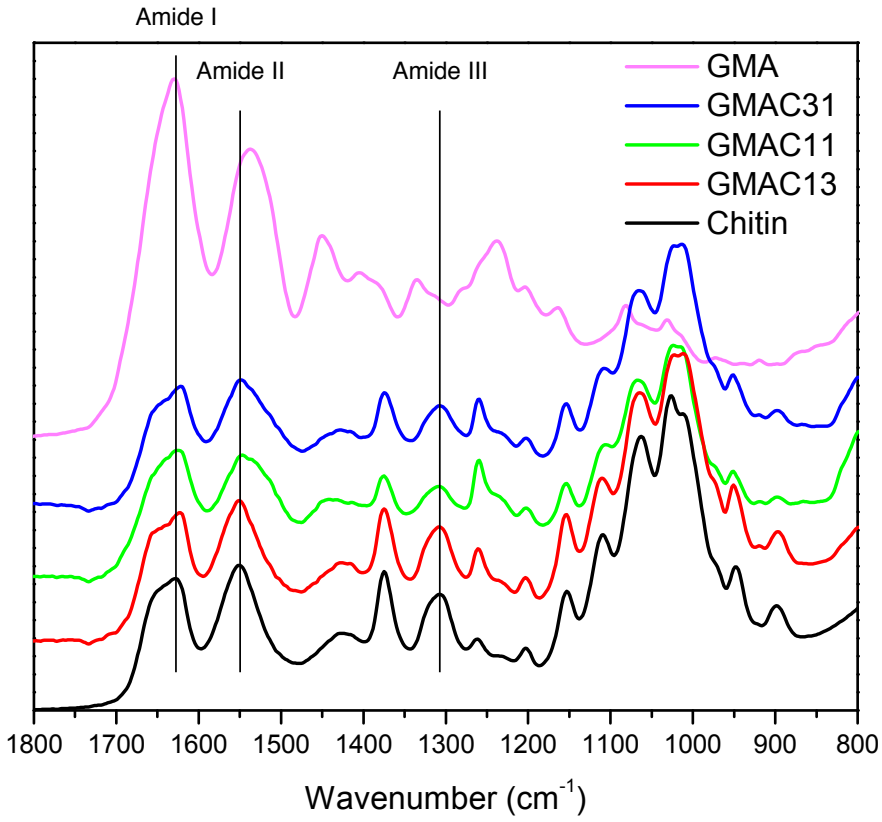

Figure 5.6. FTIR spectra of corss-linked GelMA, GMAC31, GMAC11, GMAC31, and Chitin. The spectra do not show any indication of chemical bonding between GelMA and chitin molecules. No significant change of frequency and/or intensity in major peaks of chitin (Amide I (C=O) and Amide II and III (CN-NH)) is observed.

5.4 HUVEC/MSC CO-CULTURE ANALYSIS ON GELMA-CHITIN HYDROGELS

As a proof-of-concept we co-culture HUVECs/hMSCs on GMAC13 microfabricated hydrogels cell alignment (Figure 5.7a-d). We quantify the alignment of HUVECs/hMSCs at day 3 according to the direction of the actin filaments on both patterned and non-patterned hydrogels and grouped in 10° increments (Figure 5.7e-f). For patterned hydrogels, the cells mostly align and elongate along the axis of the micropatterns with the pitch size of 12.15 μm and height of 450 nm. There is no cell alignment after 3 and 5 days on non-patterned hydrogels used as controls. For micropatterned hydrogels, over 50 % of the cells align within the 0–10° increment angle and approximately 95 % of cells are aligned with an angle < 40° respect to the direction of the micropatterns (Figure 5.7e). Unlike the patterned hydrogels, the cells randomly orient on the non-patterned control hydrogels (Figure 5.7f). Fluorescence images of cells on day 5 on either patterned or hydrogels without any patterns demonstrate formed organized networks with neighboring cells or random interconnected networks of neighboring cells (Figure 5.7c-d).

We also evaluate the viability, proliferation, and vascularization of HUVECs/hMSCs co-cultured on the GMAC13 hydrogels after 1, 3 and 5 days of culture (Figure 5.8). hMSCs are ideal cell sources for cardiovascular tissue engineering because they can differentiate into smooth muscle cells and endothelial cells *in vitro*[83, 84] and *in vivo*.[85, 86] Typically, co-culture of HUVECs and MSCs results in the formation of robust functional vascular networks within the first week.[87] On the GMAC13 hydrogels, live cells (green) attach well and exhibit a normal morphology with uniform distribution and very few dead cells (red) (Figure 5.8 a, b, c). Live/dead fluorescent staining indicates that over 90% of the cells are viable on the GMAC13 hydrogels after 1, 3 and 5 days (Figure 5.8d). HUVECs/hMSCs cells are metabolically active (PrestoBlue®) and continue to proliferate with an enhanced proliferation activity on day 5 (Figure 5.8e). To investigate the vasculogenic capacity of HUVECs/hMSCs co-culture on GMAC13 hydrogels, we study early vasculogenesis by immunostaining the expressions of the endothelial cell specific marker CD31 and early marker of smooth muscle cell differentiation, α-SMA. GMAC13 is conducive to hMSCs differentiation into smooth muscle cells (Figure 5.8f). Relative expression of CD31 by HUVECs and αSMA by hMSCs suggests a close association of hMSCs with HUVECs inducing an ongoing process of perivascular activity of cells. Consequently, the HUVECs/hMSCs co-

culture on GMAC13 is a novel platform for studying vasculogenesis that is easier to source than Matrigel[88] and more mechanically robust than collagen-based hydrogels [89].

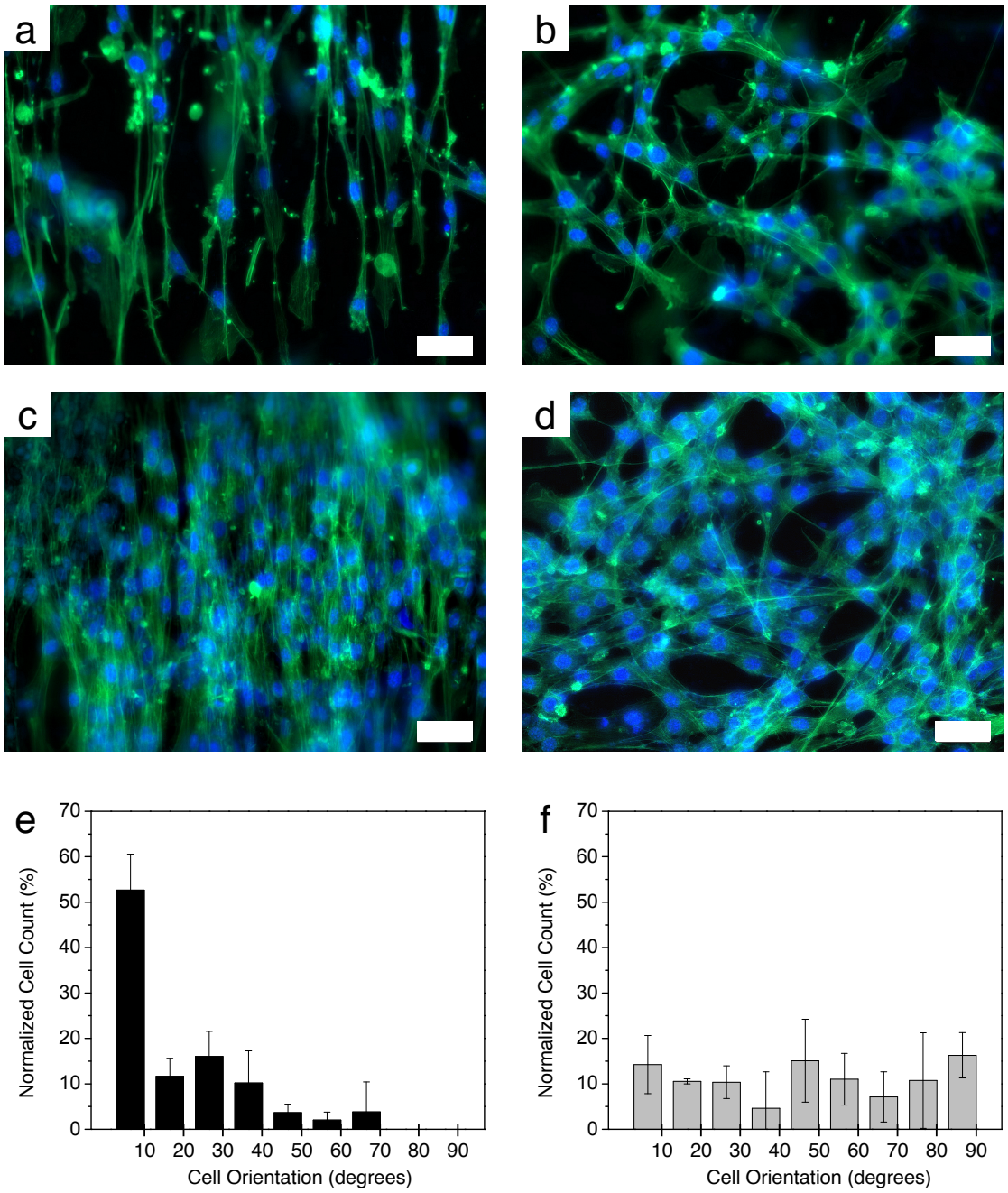

Figure 5.7. (a-d) Representative fluorescence images demonstrate Actin/Dapi stained cell orientation after 3 (a and b) and 5 days (c and d) on the patterned (a and c) and non-patterned (b and d) GMAC13 hydrogels (Scale bars=50 μm), (e and f) Normalized cell count of cellular alignment measured with respect to the longitudinal direction of the actin filaments on micropatterned GMAC13 hydrogels (e) and non-patterned GMAC13 hydrogels as control (f).

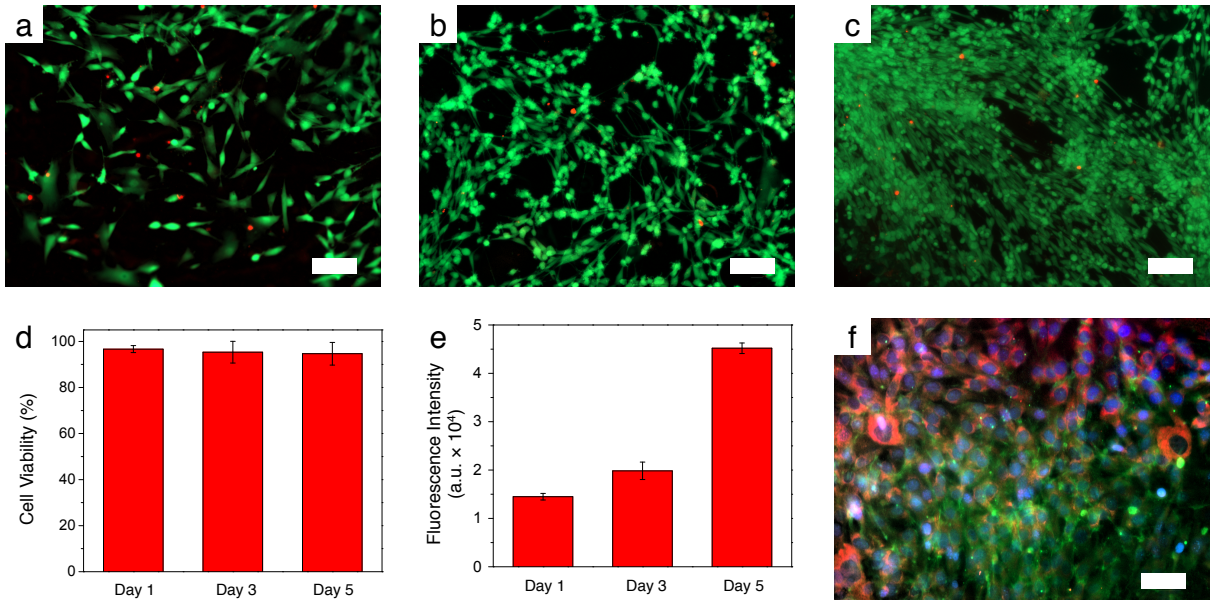

Figure 5.8. (a-c) Fluorescence microscopy images showing HUVECs/hMSCs co-culture growing on GMAC13 hydrogels after 1, 3 and 5 days, stained with Live (green) and Dead (red) viability assay kit (Scale bars represent 100 μm), (d) Quantification of cell viability on GMAC13 hydrogels after 1, 3 and 5 days, (e) PrestoBlue assay showing the proliferation of HUVECs/hMSC co-culture on GMAC13 surface after 1, 3 and 5 days, (f) Immunostaining of vascular markers for HUVECs/hMSCs grown on GMAC13 after 5 days (green: CD31, red: alpha-SMA, blue: DAPI) (scale bar represents 50 μm).

5.5 CONCLUSION

In conclusion, we report the one pot self-assembly of new crosslinked GelMA hydrogels reinforced with 3 nm chitin nanofibers (GMAC). The chitin nanofiber reinforcement increases hydrogel elastic modulus by one-thousand fold and strain to failure by > 200% improving handling and integrity for tissue engineering applications. The simple self-assembly process for these hydrogels is amenable to soft lithography strategies to create microstructures. HUVECs co-cultured with hMSCs grow, proliferate, and align on the micropatterned hydrogels and express vasculogenic markers indicating cell differentiation and formation of stable vasculature on these substrates.

5.6 MATERIALS AND METHODS

Materials: The materials and suppliers used are as follows: Squid pen chitin flakes (Industrial Research Ltd-New Zealand), hexafluoro-2-propanol (HFIP) (Oakwood Products, Inc.), gelatin type A made from porcine skin and methacrylic anhydride (MA) (Sigma-Aldrich Chemical Co., USA), 2-hydroxy-1-[4-(2-hydroxyethoxy)phenyl]-2-methyl-1-1propanone (Irgacure 2959) (Ciba Chemicals, Osaka, Japan), optical grating GE 2550-0875 Echelle Grating, 12.66 μm, 75° blaze angle (THORLABS) and polydimethylsiloxane (PDMS) (SYLGARD 184).

Preparation of GelMA-Chitin Solutions: Appropriate amounts of squid pen β-chitin aredissolved in HFIP for four days under vigorous stirring at room temperature to obtain concentration of 0.4 (w/v) %. Then, appropriate amounts of lyophilized highly methacrylated GelMA are dissolved in chitin/HFIP solution for 1 day under mild stirring at room temperature. The GelMA prepolymer is synthesized as described previously.[77] A high degree of methacrylation (~80%) is obtained by adding 8 mL of MA to 10 g of gelatin in 100 mL of Phosphate-Buffered Saline (PBS). The mixture is dialyzed in a 12-14 KDa cutoff membrane in the distilled water for one week at 40 °C and then lyophilized for one week. The GelMA-chitin solutions are GMAC31 (GelMA:chitin, 3 to 1 weight ratio), GMAC11 (1 to 1 weight ratio), and GMAC13 (1 to 3 weight ratio). The photoinitiator (PI) (Irgacure 2959) with the ratio of PI/GelMA=2 is added to each GMAC/HFIP solution and left to dissolve for 6 hrs at room temperature. The chitin/HFIP and GelMA/HFIP (PI/GeLMA = 2) solutions are also prepared by dissolving appropriate amount of each material in HFIP under stirring at room temperature for 4 days and 1 day, respectively. HFIP is a toxic

solvent and particular care is required during handling. All the above and following procedures are performed in a fume hood. In order to prepare gelatin-chitin solution, the same procedure as GelMA-chitin is used. GelMA is substituted by porcine gelatin and PI is not used.

Preparation of GelMA-Chitin and Gelatin-Chitin Hybrid Films: GelMA-chitin (GMAC), gelatin-chitin (GC), chitin and GelMA films for further measurement and testing are prepared by pouring 10 mL of each solution into a rectangular-shaped (50 × 25 mm) PDMS mold with the volume of 17.5 ml. The molds are covered by a tight parafilm with 5 holes to afford slow evaporation of the HFIP over a period of 5 days. Films obtained after shorter period of times are brittle due to increased number of defects and stress accumulated while drying. After complete drying, GMAC and GelMA films are exposed to UV irradiation (365 nm, 100W, 115V, UVP^{TM} Blak-Ray^{TM} B-100A UV Lamps) for 3 minutes in the distance of 10 cm to the lamp in dry condition to crosslink the methacrylate functional groups of GelMA. They are then washed with copious amount of DI water for 5 minutes to remove the excessive PI and uncrosslinked GelMA prepolymer. Subsequently, they dry in room temperature. The GC, chitin, and gelatin films are used for characterization as they are upon complete drying.

Preparation of Micropatterned GMAC13: The GMAC13/HFIP solution is drop cast into the master PDMS mold (replica of GE 2550-0875 Echelle Grating) to create micropatterns on top. The dried film is then exposed to UV for 3 minutes and washed with DI water for 5 min as described before.

Preparation of Hybrid Hydrogels: After washing the crosslinked GelMA and GMAC films and also patterned GMAC13 with DI water, the films are immersed in DPBS at 37 °C for 24 hrs. The hydrophilic films absorb water and swell.

Hydrogels Weight Stability Analysis: The extent of stability of GelMA and gelatin in the GMAC and GelChi hydrogels in an aqueous environment is analyzed by comparing the weight of dry hybrid films before and after immersion in DPBS at 37 °C for 24 hrs (physiological conditions) for the three weight ratios of hydrogels. Chitin and GelMA/gelatin content of the final dry films are estimated from the initial amounts considering chitin is stable and insoluble in DPBS at 37 °C for 24 hrs.

Characterization: Tapping mode Atomic Force Microscopy (AFM) is performed on a Veeco Multimode V with a Nanoscope IV controller. Veecoprobes Sb-doped Si cantilevers (ρ= 0.01-0.025 Ω-cm, k = 40 N/m, ν~ 300 kHz) are used. Fourier Transform Infrared (FTIR) spectra are

recorded with a Bruker vectex 70 FTIR spectrophotometer (4000 to 400 cm^{-1}, 4 cm^{-1} resolution) working in ATR mode. Stress vs. strain data is recorded on three rectangular samples for each material measuring 3 × 30 mm with thickness of approximately 300 μm for hydrogels. After cutting the samples with razor blade, they are examined under optical microscope to assure they do not contain any notches and major microcracks formed on the edges during cutting process. All tests are conducted with a Shimadzu AGS-X (0.1 mm/min rate) equipped with a 100 N load cell and 50 N pneumatic grips. In the case of hydrogels, a vaporizer with dual output to cover both sides of the hydrogel with some water splash on the surface is used in order to keep the humidity high (~70%) and prevent the hydrogel from drying out.

Cell Culture and Materials: Endothelial growth medium (EGM-2 BulletKit) is used to culture HUVECs. hMSCs (Lonza) are cultured in alpha-MEM medium supplemented with 10% FBS and 1% penicillin/streptomycin, 2mM L-glutamine, 1 ng/ml basic fibroblast growth factor (bFGF, Life Technologies) and 0.2 M ascorbic acid (AA, Sigma). Cells are cultured at 37 °C in a humidified atmosphere of 5% CO_2. The media are changed every two days. After the confluence is reached, cells are harvested using trypsin/EDTA and counted on a hemocytometer. Subsequently, an equal cell quantity of HUVECs and hMSCs (10^5 cells 1:1) are mixed in EGM-2, before seeding the cells on GMAC13 substrates. Sample is then placed in a multi-well plate, cultured in EGM-2 media and incubated. All experiments are performed at passages 4-8.

Cell Alignment: The alignment of cells on patterned and non-patterned GMAC13 substrates is investigated using fluorescence images based on angle of orientation with respect to the direction of the actin filaments. After culturing the HUVECs/hMSCs on the GMAC13 substrates for 3 and 5 days, the specimens are rinsed 3 times with prewarmed DPBS and fixed in 4% paraformaldehyde for 20 min at room temperature. Subsequently, the cells are washed with DPBS 3 times and permeabilized by incubating in 0.1% (w/v) Triton X-100 in DPBS for 15 min and rinsed 3 times with DPBS for 5 min. The cells are then blocked in 1% (w/v) Bovine Serum Albumin (BSA) in DPBS for 1 h, followed by staining with 1/40 dilution of Alexa Fluor 488® phalloidin (Invitrogen) in 0.1% BSA blocking solution for 2 h at room temperature to visualize F-actin. Cell nuclei are stained with 1/1000 dilution of 4'-6-Diamidino-2-phenylindole (DAPI, Invitrogen) in DPBS for 5 min. Alignment analysis is performed by measuring the deviation of

actin filaments with respect to the grooves' axis using fluorescence images (6 random images for each sample). The normalized alignment angles are grouped in 10 degrees increments to compare the orientation of cells on patterned and un-patterned samples. The analysis is performed in triplicate for each condition.

Cell Viability: Fluorescence-based LIVE/DEAD® viability/cytotoxicity assay kit (Invitrogen) consisting intracellular green-fluorescent calcein AM and red-fluorescent ethidium homodimer-1 stains is used to determine the viable and non-viable cells. The percentage of viable HUVECs/hMSCs (10^5 cells 1:1) co-cultured on the GMAC13 substrates is quantified after 1, 3, and 5 days. First a solution containing two components at 0.5 µl/ml (calcein) and 2 µl/ml (ethidium homodimer-l) are dissolved in DPBS, respectively. At each time point, the media is removed and the hydrogels covered with cells are rinsed with DPBS and subsequently 1 mL of the solution is added to each sample. Afterwards, the samples are incubated for 30 min at room temperature and then imaged with 10X magnifications using an inverted fluorescence microscope (Nikon TE 2000-U, Nikon instruments Inc., USA). The total number of cells (red and green) and number of live cells (green) are counted using ImageJ software (NIH). Finally, the cell viability is calculated and quantified by dividing live cells by total number of cells. The calculations are based on three independent samples and reported based on the mean ± standard deviation.

Cell Proliferation: Proliferation of cells is assessed using the resazurin-based PrestoBlue® assay (Invitrogen, CA), a non-toxic metabolic indicator for viable cells. Briefly, HUVECs/hMSCs co-culture (10^5 cells 1:1) are seeded on each GMAC13 substrate and incubated for 1, 3, and 5 days. After each time point the culture medium is removed and the samples are rinsed with DPBS. Subsequently, the DMEM containing 10% PrestoBlue® reagent is added to each well and incubated at 37 °C for 1 h, and the well with reagent with no cells served as the blank control. The fluorescence of the reduced PrestoBlue® dye is read at 570 (excitation) and 600 nm (emission) with a microplate reader (Biotek, USA), and all values are corrected based on blank control. Three replicates are analyzed continuously for 1, 3 and 5 days and growth were plotted based on the mean ± standard deviation.

Immunofluorescence for Vasculogenic Markers: The vasculogenic activity of HUVECs/hMSCs co-culture (10^5 cells 1:1) grown on GMAC13 substrates is investigated by immnustaining for

CD31 (Abcam, USA), and anti-Smooth Muscle Actin (α-SMA; Abcam, USA) expressions. The GMAC13 covered with cells where rinsed in DPBS and fixed in 4% paraformaldehyde solution in DPBS for 20 min. Subsequently, the cell membranes are permeabilized in 0.1% Triton X-100 in DPBS for 15 min and washed with DPBS for 3 times. The samples are then blocked with 1% (w/v) BSA in DPBS for 1 h, followed by primary antibody staining with 1/40 dilution of rabbit monoclonal anti-CD31 antibody (Abcam) and 1/100 dilution of mouse monoclonal anti-alpha smooth muscle actin antibody (Abcam) in 0.1% BSA blocking solution overnight at 4 °C. The samples are washed in DPBS three times with 1 h intervals in between the washing steps. After primary antibody staining, the samples are incubated in 1/200 dilution of Alexa Fluor-488 conjugated goat anti-rabbit (Abcam) and 1/200 dilution of Alexa Fluor-594 conjugated goat anti-mouse secondary antibodies (Abcam) in 0.1% BSA in DPBS for 2 h at room temperature. Subsequently, the samples are washed in DPBS three times with 1 h intervals in between the washing steps, followed by 1/1000 dilution DAPI staining for 5 min. After rinsing the samples with DPBS, confocal images are taken.

Chapter 6. FUTURE OUTLOOK

During my PhD research, I used HFIP to dissolve squid pen chitin flakes and self-assemble α-chitin nanofibers from aqueous Chitin/HFIP solutions. HFIP has a lot advantages over the other solvent systems I have tried such as complete dissolution of chitin, not being degradative to chitin polymer and room temperature processing condition. Also, because it is a great hydrogen bonding donor and not a good acceptor, it disrupts the hydrogen bonding between chitin chains, solubilize them, and evaporates away when exposed to open air without leaving trace in the material. However, it is a volatile corrosive liquid that can cause burns and respiratory problems in human.

The outlook of my PhD research is to replace HFIP with less harsh solvents preferably water systems. A solution of 8% NaOH/ 4% urea has been used to dissolve both cellulose and chitin[90, 91] in stable solutions by cycles of freezing and thawing. In this system, the OH^- ion disrupts intermolecular hydrogen bonding of the chitin by letting the water molecules in. The frozen water molecules expand and beak inter- and intra-sheet hydrogen bonding inside chitin chains and solubilize it. The urea stabilizes the resulting chitin chains from aggregation.

I have been successful to dissolve our squid pen chitin in the mixture of 10 g water/0.5 g urea/1g NaOH making final solution of 0.4 and 0.5 %W/V. After mixing all these materials, I put the solution in the -20°C freezer and continued with the cycles of freezing and thawing until the solution was clear. Upon thawing, I stirred the solution vigorously. Next, I dialyzed the solution in the dialysis membrane with Molecular Weight Cut Off of 3500 to dissolve away urea and NaOH. Then, I dried out the water on a mold and ended up with chitin films from the water solution. However, these films do not contain nanofibers. So, the next step would be to try to precipitate chitin nanofibers from water/chitin solution.

Using water systems to self-assemble chitin nanofiber films leads to establishment of environmentally-friendly process to make nanofiber films with great strength and stiffness and high surface area using only natural green materials and processes and with causing no harmful waste.

BIBLIOGRAPHY

1. Wan ACA, Tai BCU. CHITIN — A promising biomaterial for tissue engineering and stem cell technologies. Biotechnology Advances. (0).
2. Annabi N, Mithieux SM, Zorlutuna P, Camci-Unal G, Weiss AS, Khademhosseini A. Engineered cell-laden human protein-based elastomer. Biomaterials. 2013;34(22):5496-5505.
3. Ifuku S, Saimoto H. Chitin nanofibers: preparations, modifications, and applications. Nanoscale. 2012;4(11):3308-3318.
4. Rinaudo M. Chitin and chitosan: Properties and applications. Progress in Polymer Science. 2006;31(7):603-632.
5. Biofunctionalization of Polymers and thier Applications. Scheper PDT, editor. London New yYork: Springer Heidelberg Dordrecht; 2011.
6. Rolandi M, Rolandi R. Self-assembled chitin nanofibers and applications. Advances in Colloid and Interface Science. (0).
7. Nagahama H, Nwe N, Jayakumar R, Koiwa S, Furuike T, Tamura H. Novel biodegradable chitin membranes for tissue engineering applications. Carbohydrate Polymers. 2008;73(2):295-302.
8. While there are no methyl groups in the precursor, they are common decomposition fragments of the phenyl group.
9. Rolandi M, Rolandi R. Self-assembled chitin nanofibers and applications. Advances in Colloid and Interface Science. 2014;207(0):216-222.
10. Jayakumar R, Prabaharan M, Nair SV, Tamura H. Novel chitin and chitosan nanofibers in biomedical applications. Biotechnology Advances. 2010;28(1):142-150.
11. Lin N, Huang J, Chang PR, Anderson DP, Yu J. Preparation, Modification, and Application of Starch Nanocrystals in Nanomaterials: A Review. Journal of Nanomaterials. 2011;2011:13.
12. Muzzarelli RAA, Boudrant J, Meyer D, Manno N, DeMarchis M, Paoletti MG. Current views on fungal chitin/chitosan, human chitinases, food preservation, glucans, pectins and inulin: A tribute to Henri Braconnot, precursor of the carbohydrate polymers science, on the chitin bicentennial. Carbohydrate Polymers. 2012;87(2):995-1012.
13. Wan AC, Tai BC. CHITIN--a promising biomaterial for tissue engineering and stem cell technologies. Biotechnology advances. 2013;31(8):1776-1785.
14. Ma H, Burger C, Hsiao BS, Chu B. Ultrafine polysaccharide nanofibrous membranes for water purification. Biomacromolecules. 2011;12(4):970-976.
15. Ifuku S. Chitin and chitosan nanofibers: preparation and chemical modifications. Molecules (Basel, Switzerland). 2014;19(11):18367-18380.
16. Chen P-Y, Lin AY-M, McKittrick J, Meyers MA. Structure and mechanical properties of crab exoskeletons. Acta Biomaterialia. 2008;4(3):587-596.
17. Sarikaya M, Staley JT, Aksay IA. Processing of Ceramics by Biopolymers. Ultrastructure-Property Relationships in Biocrystals: DTIC Document; 1991Contract.
18. Ashammakhi N, Wimpenny I, Nikkola L, Yang Y. Electrospinning: Methods and Development of Biodegradable Nanofibres for Drug Release. Journal of Biomedical Nanotechnology. 2009;5(1):1-19.
19. Lee KY, Jeong L, Kang YO, Lee SJ, Park WH. Electrospinning of polysaccharides for regenerative medicine. Adv Drug Deliv Rev. 2009;61(12):1020-1032.

20. Pillai CKS, Paul W, Sharma CP. Chitin and chitosan polymers: Chemistry, solubility and fiber formation. Progress in Polymer Science. 2009;34(7):641-678.
21. Jin J, Reese V, Coler R, Carter D, Rolandi M. Chitin Microneedles for an Easy-to-Use Tuberculosis Skin Test. Advanced Healthcare Materials. 2013:n/a-n/a.
22. Cooper A, Zhong C, Kinoshita Y, Morrison RS, Rolandi M, Zhang M. Self-assembled chitin nanofiber templates for artificial neural networks. Journal of Materials Chemistry. 2012;22(7).
23. Hassanzadeh P, Kharaziha M, Nikkhah M, Shin SR, Jin J, He S, Sun W, Zhong C, Dokmeci MR, Khademhosseini A, Rolandi M. Chitin nanofiber micropatterned flexible substrates for tissue engineering. Journal of Materials Chemistry B. 2013;1(34):4217-4224.
24. Zhong C, Deng Y, Roudsari AF, Kapetanovic A, Anantram MP, Rolandi M. A polysaccharide bioprotonic field-effect transistor. Nat Commun. 2011;2:476.
25. Deng Y, Josberger E, Jin J, Rousdari AF, Helms BA, Zhong C, Anantram MP, Rolandi M. H+-type and OH--type biological protonic semiconductors and complementary devices. Sci Rep. 2013;3:2481.
26. Zhong C, Cooper A, Kapetanovic A, Fang ZH, Zhang MQ, Rolandi M. A facile bottom-up route to self-assembled biogenic chitin nanofibers. Soft Matter. 2010;6(21):5298-5301.
27. Hassanzadeh P, Sun W, de Silva JP, Jin J, Makhnejia K, Cross GLW, Rolandi M. Mechanical properties of self-assembled chitin nanofiber networks. Journal of Materials Chemistry B. 2014.
28. Hu X, Xu Z, Gao C. Multifunctional, supramolecular, continuous artificial nacre fibres. Sci Rep. 2012;2.
29. I'Anson SJ, Sampson WW. Competing Weibull and stress-transfer influences on the specific tensile strength of a bonded fibrous network. Composites Science and Technology. 2007;67(7–8):1650-1658.
30. Zussman E, Burman M, Yarin AL, Khalfin R, Cohen Y. Tensile deformation of electrospun nylon-6,6 nanofibers. Journal of Polymer Science Part B: Polymer Physics. 2006;44(10):1482-1489.
31. Inai R, Kotaki M, Ramakrishna S. Structure and properties of electrospun PLLA single nanofibres. Nanotechnology. 2005;16(2):208.
32. Aifantis K, Shrivastava S, Odegard G. Transverse mechanical properties of collagen fibers from nanoindentation. J Mater Sci: Mater Med. 2011;22(6):1375-1381.
33. Wenger MPE, Bozec L, Horton MA, Mesquida P. Mechanical Properties of Collagen Fibrils. Biophysical Journal. 2007;93(4):1255-1263.
34. Chen F, Porter D, Vollrath F. Silkworm cocoons inspire models for random fiber and particulate composites. Physical Review E. 2010;82(4):041911.
35. Zhu HX, Mills NJ, Knott JF. Analysis of the high strain compression of open-cell foams. Journal of the Mechanics and Physics of Solids. 1997;45(11–12):1875-1904.
36. Aggeli A, Nyrkova IA, Bell M, Harding R, Carrick L, McLeish TCB, Semenov AN, Boden N. Hierarchical self-assembly of chiral rod-like molecules as a model for peptide beta-sheet tapes, ribbons, fibrils, and fibers. Proceedings of the National Academy of Sciences of the United States of America. 2001;98(21):11857-11862.
37. Rowland HD, King WP, Cross GLW, Pethica JB. Measuring Glassy and Viscoelastic Polymer Flow in Molecular-Scale Gaps Using a Flat Punch Mechanical Probe. ACS Nano. 2008;2(3):419-428.

38. Cross GLW, x, Connell BS, Pethica JB, Rowland H, King WP. Variable temperature thin film indentation with a flat punch. Review of Scientific Instruments. 2008;79(1):013904-013904-013913.
39. Cheng L, Xia X, Yu W, Scriven LE, Gerberich WW. Flat-punch indentation of viscoelastic material. Journal of Polymer Science Part B: Polymer Physics. 2000;38(1):10-22.
40. Cheng Y-T, Yang F. Obtaining shear relaxation modulus and creep compliance of linear viscoelastic materials from instrumented indentation using axisymmetric indenters of power-law profiles. Journal of Materials Research. 2009;24(10):3013-3017.
41. Khademhosseini A, Langer R, Borenstein J, Vacanti JP. Microscale technologies for tissue engineering and biology. Proceedings of the National Academy of Sciences of the United States of America. 2006;103(8):2480-2487.
42. Zorlutuna P, Annabi N, Camci-Unal G, Nikkhah M, Cha JM, Nichol JW, Manbachi A, Bae H, Chen S, Khademhosseini A. Microfabricated Biomaterials for Engineering 3D Tissues. Advanced Materials. 2012;24(14):1782-1804.
43. Dvir T, Timko BP, Kohane DS, Langer R. Nanotechnological strategies for engineering complex tissues. Nature Nanotechnology. 2011;6(1):13-22.
44. Discher DE, Janmey P, Wang YL. Tissue cells feel and respond to the stiffness of their substrate. Science. 2005;310(5751):1139-1143.
45. Kaihara S, Borenstein J, Koka R, Lalan S, Ochoa ER, Ravens M, Pien H, Cunningham B, Vacanti JP. Silicon micromachining to tissue engineer branched vascular channels for liver fabrication. Tissue engineering. 2000;6(2):105-117.
46. Borenstein JT, Terai H, King KR, Weinberg EJ, Kaazempur-Mofrad MR, Vacanti JP. Microfabrication technology for vascularized tissue engineering. Biomed Microdevices. 2002;4(3):167-175.
47. Vozzi G, Flaim C, Ahluwalia A, Bhatia S. Fabrication of PLGA scaffolds using soft lithography and microsyringe deposition. Biomaterials. 2003;24(14):2533-2540.
48. King K, Wang C, Kaazempur-Mofrad M, Vacanti J, Borenstein J. Biodegradable microfluidics. Advanced Materials. 2004;16(22):2007-+.
49. Fidkowski C, Kaazempur-Mofrad MR, Borenstein J, Vacanti JP, Langer R, Wang Y. Endothelialized microvasculature based on a biodegradable elastomer. Tissue engineering. 2005;11(1-2):302-309.
50. Bettinger CJ, Langer R, Borenstein JT. Engineering substrate topography at the micro- and nanoscale to control cell function. Angewandte Chemie. 2009;48(30):5406-5415.
51. Zhao F, Veldhuis JJ, Duan Y, Yang Y, Christoforou N, Ma T, Leong KW. Low oxygen tension and synthetic nanogratings improve the uniformity and stemness of human mesenchymal stem cell layer. Mol Ther. 2010;18(5):1010-1018.
52. Zhong C, Kapetanovic A, Deng Y, Rolandi M. Nanofiber Ink: A Chitin Nanofiber Ink for Airbrushing, Replica Molding, and Microcontact Printing of Self-assembled Macro-, Micro-, and Nanostructures (Adv. Mater. 41/2011). Adv Mater. 2011;23(41):4720-4720.
53. Papadaki M, Bursac N, Langer R, Merok J, Vunjak-Novakovic G, Freed LE. Tissue engineering of functional cardiac muscle: molecular, structural, and electrophysiological studies. Am J Physiol Heart Circ Physiol. 2001;280(1):H168-178.
54. Couchman JR, Austria MR, Woods A. Fibronectin-cell interactions. J Invest Dermatol. 1990;94(6 Suppl):7S-14S.
55. Schiffman JD, Schauer CL. Cross-linking chitosan nanofibers. Biomacromolecules. 2007;8(2):594-601.

56. Zhang K, Geissler A, Fischer S, Brendler E, Baucker E. Solid-State Spectroscopic Characterization of alpha-Chitins Deacetylated in Homogeneous Solutions. Journal of Physical Chemistry B. 2012;116(15):4584-4592.
57. Feinberg AW, Feigel A, Shevkoplyas SS, Sheehy S, Whitesides GM, Parker KK. Muscular thin films for building actuators and powering devices. Science. 2007;317(5843):1366-1370.
58. Lovett M, Lee K, Edwards A, Kaplan DL. Vascularization strategies for tissue engineering. Tissue Eng Part B Rev. 2009;15(3):353-370.
59. Engelmayr GC, Cheng M, Bettinger CJ, Borenstein JT, Langer R, Freed LE. Accordion-like honeycombs for tissue engineering of cardiac anisotropy. Nature materials. 2008;7(12):1003-1010.
60. Dvir T, Timko BP, Brigham MD, Naik SR, Karajanagi SS, Levy O, Jin H, Parker KK, Langer R, Kohane DS. Nanowired three-dimensional cardiac patches. Nat Nano. 2011;6(11):720-725.
61. Annabi N, Tsang K, Mithieux SM, Nikkhah M, Ameri A, Khademhosseini A, Weiss AS. Highly Elastic Micropatterned Hydrogel for Engineering Functional Cardiac Tissue. Advanced Functional Materials. 2013:n/a-n/a.
62. Shigemasa Y, Matsuura H, Sashiwa H, Saimoto H. Evaluation of different absorbance ratios from infrared spectroscopy for analyzing the degree of deacetylation in chitin. International Journal of Biological Macromolecules. 1996;18(3):237-242.
63. Nikkhah M, Eshak N, Zorlutuna P, Annabi N, Castello M, Kim K, Dolatshahi-Pirouz A, Edalat F, Bae H, Yang Y, Khademhosseini A. Directed endothelial cell morphogenesis in micropatterned gelatin methacrylate hydrogels. Biomaterials. 2012;33(35):9009-9018.
64. Jin J, Hassanzadeh P, Perotto G, Sun W, Brenckle MA, Kaplan D, Omenetto FG, Rolandi M. A Biomimetic Composite from Solution Self-Assembly of Chitin Nanofibers in a Silk Fibroin Matrix. Advanced Materials. 2013;25(32):4482-4487.
65. Vincent JFV. Arthropod cuticle: a natural composite shell system. Composites Part a-Applied Science and Manufacturing. 2002;33(10):1311-1315.
66. Fratzl P, Weinkamer R. Nature's hierarchical materials. Progress in Materials Science. 2007;52(8):1263-1334.
67. Jang M-K, Kong B-G, Jeong Y-I, Lee CH, Nah J-W. Physicochemical characterization of α-chitin, β-chitin, and γ-chitin separated from natural resources. Journal of Polymer Science Part A: Polymer Chemistry. 2004;42(14):3423-3432.
68. Falini G, Weiner S, Addadi L. Chitin-silk fibroin interactions: Relevance to calcium carbonate formation in invertebrates. Calcified Tissue International. 2003;72(5):548-554.
69. Hu X, Kaplan D, Cebe P. Determining Beta-Sheet Crystallinity in Fibrous Proteins by Thermal Analysis and Infrared Spectroscopy. Macromolecules. 2006;39(18):6161-6170.
70. Fu S-Y, Lauke B. The elastic modulus of misaligned short-fiber-reinforced polymers. Composites Science and Technology. 1998;58(3–4):389-400.
71. Springer handbook of crystal growth. 1st ed. New York: Springer; 2009.
72. Khademhosseini A, Langer R. Microengineered hydrogels for tissue engineering. Biomaterials. 2007;28(34):5087-5092.
73. Xiao W, He J, Nichol JW, Wang L, Hutson CB, Wang B, Du Y, Fan H, Khademhosseini A. Synthesis and characterization of photocrosslinkable gelatin and silk fibroin interpenetrating polymer network hydrogels. Acta Biomater. 2011;7(6):2384-2393.

74. Ahadian S, Ramón-Azcón J, Estili M, Liang X, Ostrovidov S, Shiku H, Ramalingam M, Nakajima K, Sakka Y, Bae H, Matsue T, Khademhosseini A. Hybrid hydrogels containing vertically aligned carbon nanotubes with anisotropic electrical conductivity for muscle myofiber fabrication. Sci Rep. 2014;4.
75. Kopeček J. Hydrogel Biomaterials: A Smart Future? Biomaterials. 2007;28(34):5185-5192.
76. Nichol JW, Koshy ST, Bae H, Hwang CM, Yamanlar S, Khademhosseini A. Cell-laden microengineered gelatin methacrylate hydrogels. Biomaterials. 2010;31(21):5536-5544.
77. Van Den Bulcke AI, Bogdanov B, De Rooze N, Schacht EH, Cornelissen M, Berghmans H. Structural and Rheological Properties of Methacrylamide Modified Gelatin Hydrogels. Biomacromolecules. 2000;1(1):31-38.
78. Zhao X, Lang Q, Yildirimer L, Lin ZY, Cui W, Annabi N, Ng KW, Dokmeci MR, Ghaemmaghami AM, Khademhosseini A. Photocrosslinkable Gelatin Hydrogel for Epidermal Tissue Engineering. Advanced Healthcare Materials. 2015:n/a-n/a.
79. Hassanzadeh P, Sun W, DeSilva J, Jin J, Makhnejia K, Cross G, Rolandi M. Mechanical Properties of Self-Assembled Chitin Nanofiber Networks. Journal of Materials Chemistry B. 2013.
80. Jin J, Reese V, Coler R, Carter D, Rolandi M. Chitin Microneedles for an Easy-to-Use Tuberculosis Skin Test. Advanced Healthcare Materials. 2014;3(3):349-353.
81. Rolandi M, Rolandi R. Self-assembled chitin nanofibers and applications. Advances in Colloid and Interface Science. 2014;207:216-222.
82. Zhong C, Kapetanovic A, Deng YX, Rolandi M. A Chitin Nanofiber Ink for Airbrushing, Replica Molding, and Microcontact Printing of Self-assembled Macro-, Micro-, and Nanostructures. Advanced Materials. 2011;23(41):4776-+.
83. Oswald J, Boxberger S, Jorgensen B, Feldmann S, Ehninger G, Bornhauser M, Werner C. Mesenchymal stem cells can be differentiated into endothelial cells in vitro. Stem Cells. 2004;22(3):377-384.
84. Cho S-W, Lim SH, Kim I-K, Hong YS, Kim S-S, Yoo KJ, Park H-Y, Jang Y, Chang BC, Choi CY, Hwang K-C, Kim B-S. Small-Diameter Blood Vessels Engineered With Bone Marrow–Derived Cells. Annals of Surgery. 2005;241(3):506-515.
85. Sutherland FW, Perry TE, Yu Y, Sherwood MC, Rabkin E, Masuda Y, Garcia GA, McLellan DL, Engelmayr GC, Jr., Sacks MS, Schoen FJ, Mayer JE, Jr. From stem cells to viable autologous semilunar heart valve. Circulation. 2005;111(21):2783-2791.
86. Matsumura G, Miyagawa-Tomita S, Shin'oka T, Ikada Y, Kurosawa H. First evidence that bone marrow cells contribute to the construction of tissue-engineered vascular autografts in vivo. Circulation. 2003;108(14):1729-1734.
87. Jeon JS, Bersini S, Gilardi M, Dubini G, Charest JL, Moretti M, Kamm RD. Human 3D vascularized organotypic microfluidic assays to study breast cancer cell extravasation. Proceedings of the National Academy of Sciences. 2015;112(1):214-219.
88. Kleinman HK, Martin GR. Matrigel: Basement membrane matrix with biological activity. Seminars in Cancer Biology. 2005;15(5):378-386.
89. Helary C, Bataille I, Abed A, Illoul C, Anglo A, Louedec L, Letourneur D, Meddahi-Pellé A, Giraud-Guille MM. Concentrated collagen hydrogels as dermal substitutes. Biomaterials. 2010;31(3):481-490.
90. Hu XW, Du YM, Tang YF, Wang Q, Feng T, Yang JH, Kennedy JF. Solubility and property of chitin in NaOH/urea aqueous solution. Carbohydrate Polymers. 2007;70(4):451-458.

91. Zheng H, Zhou JP, Du YM, Zhang LN. Cellulose/chitin films blended in NaOH/urea aqueous solution. Journal of Applied Polymer Science. 2002;86(7):1679-1683.

VITA

Pegah Hassanzadeh was born in a small industrial city, Arak, Iran. She moved to Tehran, the capital, when she was 10 years old and graduated from high school with the focus of mathematics and physics in 2004. She then graduated with a BS in Materials (Ceramics) Engineering from Iran University of Science and Technology, Tehran, Iran, in 2009. In July 2010, she came to United States and started her studies in Biomedical Materials Engineering Science at Alfred University focusing on injectable biomaterials for wound healing applications. She then graduated with a MS from Alfred University in May 2012. Her MS work has resulted in two journal papers and two conference papers. Pegah has been awarded "The Korean Alumni Association of Alfred University Award" for Outstanding International Graduate Student in 2012.

In the next step, she joined University of Washington to pursue her PhD in Materials Science and Engineering under the supervision of Prof. Rolandi in June 2012. She has worked on bio-inspired chitin nanofiber films chemistry, processing and mechanical properties for various applications including biomedical and regenerative medicine. During her PhD, she has been awarded the Dean's Fellowship by College of Engineering (COE) in 2013 and the Outstanding Female Engineer Award by Society of Women Engineers (SWE) in 2014. She has been also recipient of several travel grants from University of Washington to attend Materials Research Society (MRS) meeting and exhibition and the International Conference on Mechanics of Biomaterials and Tissues (ICMOBT). In December 2015, she graduated with a Doctor of Philosophy in Materials Science and Engineering-Nanotechnology and Molecular Engineering (NTME)-dual degree from the University of Washington.